Vessel-Specific Reintroduction of CINNAMOYL-COA REDUCTASE1 (CCR1) in Dwarfed *ccr1* Mutants Restores Vessel and Xylary Fiber Integrity and Increases Biomass[1][OPEN]

Barbara De Meester,[a,b] Lisanne de Vries,[a,b] Merve Özparpucu,[c,d] Notburga Gierlinger,[e] Sander Corneillie,[a,b] Andreas Pallidis,[a,b] Geert Goeminne,[a,b,f] Kris Morreel,[a,b,f] Michiel De Bruyne,[a,b] Riet De Rycke,[a,b] Ruben Vanholme,[a,f,2] and Wout Boerjan[a,b,f,2,3]

[a]Department of Plant Biotechnology and Bioinformatics, Ghent University, B-9052 Ghent, Belgium
[b]VIB Center for Plant Systems Biology, B-9052 Ghent, Belgium
[c]Institute for Building Materials, Swiss Federal Institute of Technology Zürich, 8093 Zuerich, Switzerland
[d]Applied Wood Materials, Swiss Federal Laboratories of Materials Science and Technology, 8600 Duebendorf, Switzerland
[e]Institute for Biophysics, University of Natural Resources and Life Sciences Vienna, 1190 Vienna, Austria
[f]VIB Metabolomics Core, B-9052 Ghent, Belgium

ORCID IDs: 0000-0003-2485-330X (B.D.M.); 0000-0002-3245-9081 (L.d.V.); 0000-0003-3039-0129 (S.C.); 0000-0002-3699-9931 (N.G.); 0000-0001-7680-912X (A.P.); 0000-0002-0337-2999 (G.G.); 0000-0002-3121-9705 (K.M.); 0000-0002-1276-1857 (M.D.B.); 0000-0001-8270-7015 (R.D.R.); 0000-0001-5848-3138 (R.V.); 0000-0003-1495-510X (W.B.).

Lignocellulosic biomass is recalcitrant toward deconstruction into simple sugars due to the presence of lignin. To render lignocellulosic biomass a suitable feedstock for the bio-based economy, plants can be engineered to have decreased amounts of lignin. However, engineered plants with the lowest amounts of lignin exhibit collapsed vessels and yield penalties. Previous efforts were not able to fully overcome this phenotype without settling in sugar yield upon saccharification. Here, we reintroduced *CINNAMOYL-COENZYME A REDUCTASE1* (*CCR1*) expression specifically in the protoxylem and metaxylem vessel cells of Arabidopsis (*Arabidopsis thaliana*) *ccr1* mutants. The resulting *ccr1 ProSNBE:CCR1* lines had overcome the vascular collapse and had a total stem biomass yield that was increased up to 59% as compared with the wild type. Raman analysis showed that monolignols synthesized in the vessels also contribute to the lignification of neighboring xylary fibers. The cell wall composition and metabolome of *ccr1 ProSNBE:CCR1* still exhibited many similarities to those of *ccr1* mutants, regardless of their yield increase. In contrast to a recent report, the yield penalty of *ccr1* mutants was not caused by ferulic acid accumulation but was (largely) the consequence of collapsed vessels. Finally, *ccr1 ProSNBE:CCR1* plants had a 4-fold increase in total sugar yield when compared with wild-type plants.

Lignocellulose, being the most abundant biomass on earth, has great potential as a renewable feedstock for the production of carbon-neutral chemicals and polymers in the bio-based economy (Vanholme et al., 2013a; Isikgor and Becer, 2015). Lignocellulosic biomass is composed mainly of secondary thickened cell walls, which primarily consist of cellulose and hemicellulose polysaccharides, impregnated with lignins (Cosgrove, 2005). The latter are aromatic heteropolymers, composed mainly of *p*-hydroxyphenyl (H), guaiacyl (G), and syringyl (S) units, derived from the monolignols *p*-coumaryl, coniferyl, and sinapyl alcohol, respectively (Boerjan et al., 2003; Vanholme et al., 2010). Lignin provides the plant with the necessary strength and hydrophobicity in order to stand upright and transport water through the vascular system (Weng and Chapple, 2010). In addition, it acts as a physical barrier against pathogens and herbivores (Weng and Chapple, 2010; Miedes et al., 2014). Unfortunately, lignin also is the

major limiting factor in the processing of lignocellulosic biomass for downstream applications (Chen and Dixon, 2007; Van Acker et al., 2013; Vanholme et al., 2013b). This aromatic polymer contributes to the recalcitrance of the plant cell wall toward deconstruction by hindering the enzymatic hydrolysis of cell wall polysaccharides into simple sugars (i.e. saccharification; Weng et al., 2008; Pauly and Keegstra, 2010). Therefore, several efforts to reduce cell wall recalcitrance have focused on modifying the lignin content and/or composition (Goujon et al., 2003; Chen and Dixon, 2007; Leplé et al., 2007; Shadle et al., 2007; Jackson et al., 2008; Day et al., 2009; Voelker et al., 2010; Eudes et al., 2012, 2015, 2016; Mansfield et al., 2012; Wilkerson et al., 2014; Mottiar et al., 2016).

Lignin-modified plants that show the highest improvement in saccharification efficiency typically suffer from undesired phenotypes, including biomass and seed yield penalties, a phenomenon also called lignin modification-induced dwarfism (Chen and Dixon, 2007; Shadle et al., 2007; Bonawitz and Chapple, 2013; Van Acker et al., 2013, 2014; Vanholme et al., 2013b). Although the molecular mechanisms for lignin modification-induced dwarfism are still poorly understood, several hypotheses have been postulated to explain this phenomenon. First, the dwarfed phenotype of lignin-modified plants could be caused by the loss of vessel cell wall integrity, which, in turn, results in the inability of the plant to efficiently transport nutrients and water from the roots to the aerial parts. As a consequence, a collapse of the weakened vessel cells occurs under the negative pressure generated by transpiration, which is called the *irregular xylem* (*irx*) phenotype (Bonawitz and Chapple, 2013). For example, irregular vessels have been reported for different plant species (Arabidopsis [*Arabidopsis thaliana*], poplar [*Populus tremula × Populus alba*], and tobacco [*Nicotiana tabacum*]) perturbed in the expression of the lignin biosynthesis genes *PHENYLALANINE AMMONIA-LYASE* (*PAL*; Huang et al., 2010), *CINNAMATE 4-HYDROXYLASE* (*C4H*; Stout and Chapple, 2004), *4-COUMARATE: COENZYME A LIGASE* (*4CL*; Voelker et al., 2010), *HYDROXYCINNAMOYL-COENZYME A SHIKIMATE/ QUINATE HYDROXYCINNAMOYL TRANSFER-ASE* (*HCT*; Besseau et al., 2007), *p-COUMARATE 3-HYDROXYLASE* (*C3H*; Franke et al., 2002), *CAFFEOYL SHIKIMATE ESTERASE* (*CSE*; Vanholme et al., 2013b), *CAFFEOYL-COENZYME A O-METHYLTRANSFERASE* (*CCoAOMT*; Zhong et al., 1998), and *CINNAMOYL-COENZYME A REDUCTASE* (*CCR*; Piquemal et al., 1998; Jones et al., 2001). Furthermore, a series of dwarfed cellulose and hemicellulose biosynthesis mutants also exhibit the *irx* phenotype (Turner and Somerville, 1997; Taylor et al., 1999; Brown et al., 2005; Persson et al., 2007; Li et al., 2012).

A second (or additional) cause for the observed yield penalties could be the accumulation of pathway intermediates (or derivatives thereof) that could be toxic for the plant. For example, *ccr1* mutants show strongly increased levels of ferulic acid, which was described to drastically decrease the levels of reactive oxygen species (ROS; Xue et al., 2015). Because high levels of ROS are required for the exit from cell proliferation, the defective cell cycle and dwarfed growth of *ccr1* mutants have been ascribed to the high levels of ferulic acid leading to reduced levels of ROS (Xue et al., 2015).

A third hypothesis explaining the yield penalty of lignin-modified plants could be the depletion of other phenylpropanoid-related metabolites that are essential for normal plant development (Bonawitz and Chapple, 2013).

Fourth, the triggering of an active cell wall integrity pathway, which allows plants to sense cell wall abnormalities, could result in transcriptional responses that, in turn, cause growth perturbations (Vanholme et al., 2012; Bonawitz and Chapple, 2013). Such transcriptional control mechanisms of the phenylpropanoid metabolism have been shown to be involved in the response to lignin pathway perturbations (Bonawitz et al., 2014; Anderson et al., 2015). More specifically, mutation of genes encoding subunits of the transcriptional coregulatory complex Mediator (Med5A and Med5B) resulted in a (partial) reversion of the growth penalty, the reduced lignin abundance, and the collapsed vessels of *c3h1* mutants (Bonawitz et al., 2014).

Efforts have been made to overcome the dwarfed phenotype of lignin mutants while maintaining the beneficial high sugar yield upon saccharification. Some of these attempts focused on the recovery of vessel cell integrity in lignin mutants. In these studies, *VASCULAR-RELATED NAC DOMAIN6* (*VND6*) and *VND7* promoter sequences were used to drive the expression of a lignin biosynthesis gene in the respective lignin mutant, thereby aiming at reintroducing lignin biosynthesis specifically in vessel cells. The expression of *VND6* has been shown to be restricted to the metaxylem vessels, whereas *VND7* had the highest expression level in protoxylem vessels (Kubo et al., 2005; Zhong et al., 2008; Vargas et al., 2016). An example of this strategy includes the partial restoration of the dwarfed phenotype of *c4h* knockdown mutants by the reintroduction of the *C4H* gene under the control of a 2,757-bp *VND6* promoter sequence, resulting in plants with normal, open vessels (Yang et al., 2013). However, *c4h ProVND6:C4H* plants showed a reoccurrence of lignin in the interfascicular fiber region, indicating that the complementation strategy used was not highly specific for vessel cells. Moreover, these lines had lower sugar yields per mg of cell wall when compared with *c4h* mutants. A similar strategy has been used in Arabidopsis *cse-2* mutants (Vargas et al., 2016). Here, introducing *CSE* under the control of a 1,004-bp *VND6* or 1,997-bp *VND7* promoter sequence partially restored their growth and vascular integrity. However, the specific reoccurrence of lignin in the xylem, and not in the interfascicular fibers, of *cse-2 ProVND6:CSE* and *cse-2 ProVND7:CSE* lines resulted in cellulose-to-glucose conversion efficiencies equal to those of *cse-2* mutants. Similar results were obtained for a vessel-specific complementation approach of xylan mutants, where the use of 2,757-bp *VND6* and 2,009-bp *VND7*

promoter sequences only partially recovered the *irx* and dwarfed phenotype of the respective xylan biosynthesis mutants (Petersen et al., 2012). Taken together, these data hint that the *VND6* and *VND7* promoters are not strong and/or not specific enough to fully restore the yield penalty and at the same time keep the high cellulose-to-glucose conversion efficiency of cell wall biosynthesis mutants.

Here, we completely overcame the total plant biomass penalty of severely dwarfed *ccr1* mutants without lowering general ferulic acid levels but while fully maintaining its high saccharification potential. To achieve this, the artificial *SECONDARY WALL NAC BINDING ELEMENT* of the *XYLEM CYSTEINE PROTEASE1* promoter (*ProSNBE*) was chosen to drive the expression of the *CCR1* gene in a *ccr1* mutant background (McCarthy et al., 2011). *ProSNBE* is bound by both VND6 and VND7 and confers expression in both protoxylem and metaxylem vessels (Zhong et al., 2010). The resulting *ccr1 ProSNBE:CCR1* lines showed a full recovery in vascular integrity, a strong increase in total stem biomass as compared with wild-type plants, and provided evidence for monolignol transport from vessel cells to the cell wall of xylary fibers.

RESULTS

ProSNBE Confers Vessel-Specific Expression in Both the Protoxylem and Metaxylem of Arabidopsis

To fully restore the integrity of the vessels and the growth of *ccr1* mutants, a vessel-specific promoter was required that conferred higher expression levels and/or a broader expression pattern than the previously tested *VND6* and *VND7* promoters (Petersen et al., 2012; Yang et al., 2013; Vargas et al., 2016). The artificial *ProSNBE* has been shown to direct the expression of reporter genes to xylem vessel cells of the Arabidopsis inflorescence stem (McCarthy et al., 2011). Furthermore, *ProSNBE* should confer expression in both protoxylem and metaxylem vessels, because it is bound by both VND6 and VND7 (Zhong et al., 2010). The *ProSNBE* used here is composed of three tandem repeats of the cis-regulatory *SNBE1* originating from the Arabidopsis *XYLEM CYSTEINE PROTEASE1* (*XCP1*) promoter, fused to the cauliflower mosaic virus (CaMV) *35S* minimal promoter (Fig. 1). The *XCP1* gene has been shown to be expressed specifically in Arabidopsis vessel cells, where the corresponding protein is involved in vessel autolysis during xylogenesis (Ohashi-Ito et al., 2010; Zhong et al., 2010; McCarthy et al., 2011).

To investigate whether *ProSNBE* indeed specifically directs gene expression in the vessels throughout the xylem (including protoxylem and metaxylem), we fused *ProSNBE* to the *GFP* and *GUS* reporter genes and studied the expression pattern in various organs of transformed Arabidopsis plants. In roots, *GFP* expression was observed in the xylem vessel cells (Fig. 1). In inflorescence stems, GUS staining was detected in the xylem, but it was lacking in interfascicular fibers or

pith cells (Fig. 1). Detailed examination of *ProSNBE:GFP:GUS* lines revealed GUS activity in developing vessels of both protoxylem and metaxylem (Fig. 1; Supplemental Fig. S1). In addition, GUS activity was found in the vasculature of siliques, flowers, and rosette leaves (Fig. 1). As described for *ProXCP1:GUS* plants, the GUS activity of *ProSNBE:GFP:GUS* plants appeared to be discontinuous throughout the vasculature, with cells lacking GUS activity alternating with those showing GUS activity (Fig. 1; Funk et al., 2002). This discontinuous staining pattern could be a reflection of the degradation of the GUS protein at the vacuole or protoplast degeneration stage occurring during vessel maturation. As a result, cells that passed this stage will lack the GUS signal. Because *ProSNBE* was found to restrict expression to both the protoxylem and metaxylem vessel cells, this promoter was used further for the envisioned complementation strategy.

The Reintroduction of *CCR1* Expression under the Control of *ProSNBE* Restores the Dwarfed Phenotype of *ccr1* Mutants

To restrict lignin biosynthesis to the vessel cells, *ProSNBE* was used to drive expression of the *CCR1* gene in both *ccr1-3* and *ccr1-6* mutant backgrounds. Two independent, homozygous and single-locus *ccr1-3* and *ccr1-6* lines harboring the *ProSNBE:CCR1* construct were selected and used for further analyses. To first evaluate whether the *ProSNBE:CCR1* constructs successfully restored plant growth, the *ccr1 ProSNBE:CCR1* lines were grown alongside their respective *ccr1* background and the wild type under short-day conditions for 6 weeks, after which they were moved to long-day conditions. These growth conditions allowed the development of large rosettes and tall inflorescence stems to maximize secondary cell wall thickening (Vanholme et al., 2012). Whereas the *ccr1* rosettes were smaller when compared with the wild type, the rosette size was fully recovered in *ccr1 ProSNBE:CCR1* plants (Fig. 2). The final height of the primary inflorescence stem of *ccr1 ProSNBE:CCR1* lines was equal to that of the wild type and approximately 2-fold higher than that of their respective *ccr1* mutants (Fig. 2; Table I). The final dry weight of the primary (main) inflorescence stem (devoid of siliques and leaves) of both *ccr1-6 ProSNBE:CCR1* lines and *ccr1-3 ProSNBE:CCR1* line 2 was not significantly different from that of the wild type, whereas all four lines were significantly heavier (78%–124%) than their respective *ccr1* background (Table I). The final dry weight of the primary inflorescence stem of *ccr1-3 ProSNBE:CCR1* line 1 was even increased (by 19%) when compared with that of the wild type (Table I).

Although the *ccr1 ProSNBE:CCR1* plants were recovered in rosette and primary inflorescence stem biomass, some phenotypic differences from the wild type were noted. First, it was observed that the *ccr1 ProSNBE:CCR1* plants had more secondary inflorescence
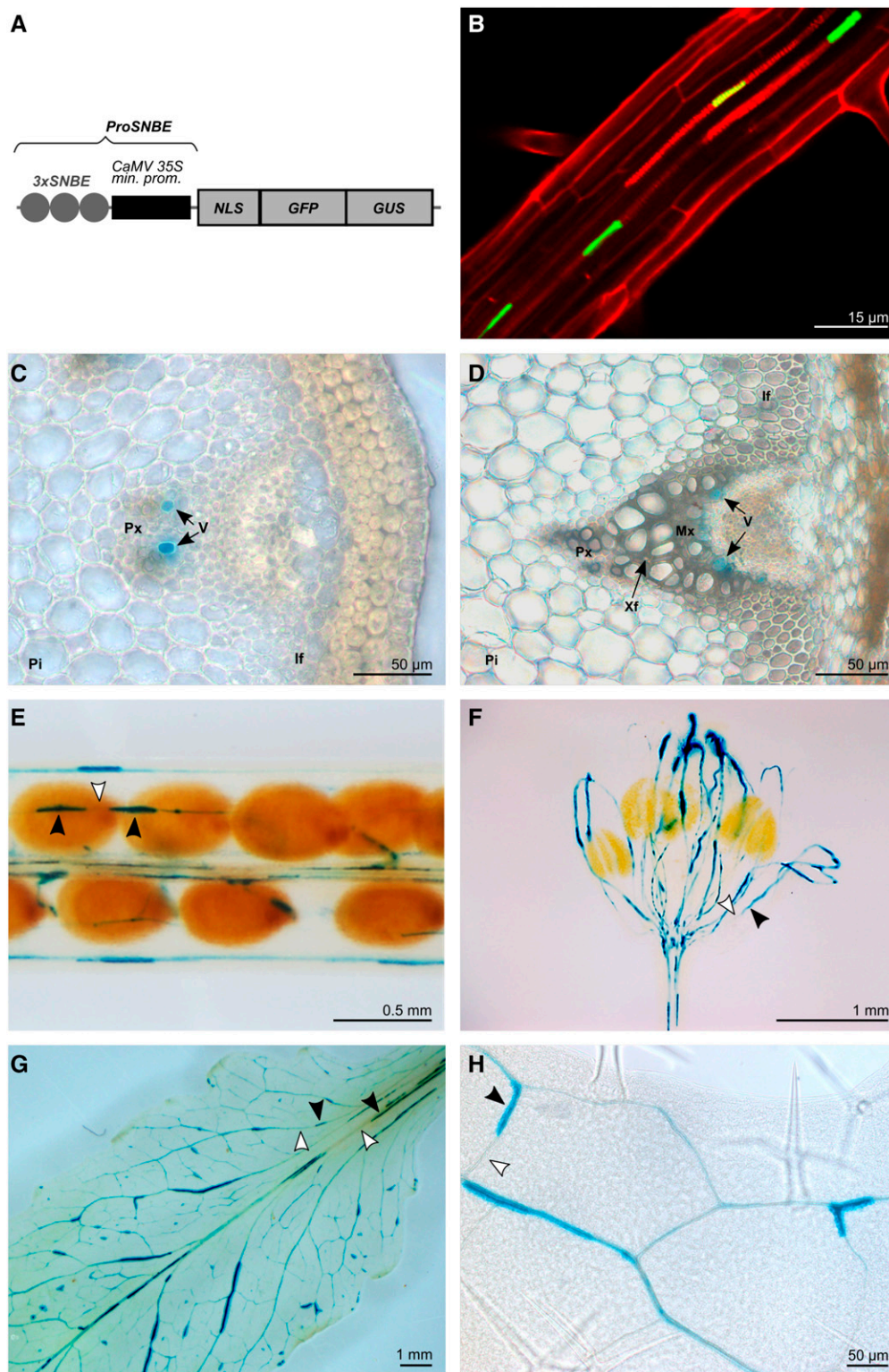
Figure 1. Expression pattern conferred by *ProSNBE*. A, Diagram of the *ProSNBE*:*GFP*:*GUS* construct: *GFP* and *GUS* reporter genes are driven by three copies of the *XCP1-SNBE* sequence fused to the CaMV minimal 35S promoter (*ProSNBE*). NLS, Nuclear localization signal. B, Expression analysis in roots showing GFP in xylary vessels. Propidium iodide was used to counterstain the cell wall. C, Cross section of an elongating internode of the primary inflorescence stem showing GUS staining in developing vessels of the protoxylem. D, Cross section of a nonelongating internode of the primary inflorescence stem showing GUS staining in developing vessels of the metaxylem but not in xylary or interfascicular fibers. E to H, *GUS* expression analysis in siliques (E),

stems in comparison with the wild type (Fig. 2). Hence, we determined the weight and number of secondary inflorescence stems originating (1) from the rosette and (2) directly from the primary inflorescence stem. The *ccr1 ProSNBE:CCR1* plants had more secondary inflorescence stems originating from the rosette and an increase in secondary inflorescence stem biomass of 49% to 75% in comparison with the wild type (Table I). The increase in the number of secondary inflorescences was also observed in *ccr1-6* mutants but not in the *ccr1-3* mutants (Table I). In comparison with that of the wild type, *ccr1-3* and *ccr1-6* total (primary and secondary) stem biomass was reduced by 45% and 22%, respectively, whereas the *ccr1 ProSNBE:CCR1* plants had an increase of 38% to 59% in total stem biomass (Table I).

A second phenotypic difference between *ccr1 ProSNBE:CCR1* lines and the wild type was a perturbation in seed development in *ccr1 ProSNBE:CCR1* lines. Confirming previous observations (Mir Derikvand et al., 2008), *ccr1-3* and *ccr1-6* mutants had a lower number of seeds when compared with the wild type (−90% and −82%, respectively; Table I). The total seed mass was reduced by 89% and 76%, respectively, whereas the individual seeds were heavier (+27% and +25%, respectively) when compared with the wild type (Table I). Although less severe than their respective *ccr1* backgrounds, the *ccr1-3 ProSNBE:CCR1* and *ccr1-6 ProSNBE:CCR1* lines still had a lower number of seeds (−49% and −54%, respectively) when compared with the wild type (Table I). The total seed biomass in these lines was decreased by 45% and 30%, respectively, and the seeds were slightly heavier (+14% and +21%, respectively) when compared with the wild type (Table I). The total plant biomass (aerial part of the plant, without the rosette) of the *ccr1 ProSNBE:CCR1* lines was equal or higher when compared with the wild type, whereas that of *ccr1* was reduced significantly to more than half that of the wild type (Table I). Because the *ccr1-3 ProSNBE:CCR1* lines and *ccr1-6 ProSNBE:CCR1* lines were phenotypically similar (Table I; Fig. 2), we decided to focus further efforts mainly on the analysis of the *ccr1-6 ProSNBE:CCR1* lines.

We hypothesized that the increase in the number of secondary inflorescence stems, and hence the total stem biomass, could have been a secondary consequence of the impaired seed development in the *ccr1 ProSNBE:CCR1* lines. To test this hypothesis, immature siliques were systematically removed throughout development, with a frequency of three times per week. As has been described before, the removal of siliques resulted in delayed senescence and the outgrowth of more secondary inflorescences for all lines examined compared

with the control (in which all lines were grown without the removal of siliques; Supplemental Table S1; Hensel et al., 1994; Wuest et al., 2016). The *ccr1-6 ProSNBE:CCR1* lines were now equal to the wild type in both the number of secondary inflorescences (originating from both the rosette and the main stem) and the total stem biomass (Table II). These results suggest a role for seed development signals in the increase of lignocellulosic biomass in the *ccr1 ProSNBE:CCR1* lines.

ProSNBE:CCR1 Reinforces the Vascular System and Partially Restores Lignin Deposition in the Xylem of *ccr1* Mutants

To examine whether the vessel-specific expression of *CCR1* in *ccr1* leads to vessel-specific lignification and restoration of vessel integrity, the lignin of fully grown wild-type, *ccr1*, and *ccr1 ProSNBE:CCR1* plants was visualized with Wiesner and Mäule staining and via autofluorescence (Fig. 3; Supplemental Fig. S2). In the wild type, the xylem tissue, which contains large, open vessels, and the interfascicular fibers were heavily lignified. In accordance with previous reports (Jones et al., 2001; Goujon et al., 2003; Mir Derikvand et al., 2008), *ccr1* mutants showed an overall reduction in lignin deposition and developed irregularly shaped and collapsed vessels. The xylem tissue of the *ccr1 ProSNBE:CCR1* lines showed a strong coloration and contained large open vessels, similar to those of the wild type. Remarkably, both vessels and xylary fibers of *ccr1 ProSNBE:CCR1* lines appeared to be lignified. On the other hand, the interfascicular fibers of the *ccr1 ProSNBE:CCR1* lines showed reduced lignin deposition similar to *ccr1* mutants.

Because the previously described lignin visualization methods do not allow visualization of the anatomical features of the secondary cell walls, transmission electron microscopy was performed on the different lines (Fig. 4). The secondary cell walls of the vessels and (xylary and interfascicular) fibers of wild-type stems were organized, compact, and displayed good cohesion. By contrast, the *ccr1-6* mutant exhibited dramatic disorganization and loosening of the secondary walls in both vessels and fibers. The xylem tissue of *ccr1-6 ProSNBE:CCR1* lines appeared similar to that of the wild type, indicated by its proper organization and internal cohesion of the walls in both the vessels and xylary fibers. However, the phenotype of the interfascicular fibers of *ccr1-6 ProSNBE:CCR1* appeared to be similar to that of *ccr1-6*, indicated by the loosening of the secondary cell wall. Additionally, the interfascicular

Figure 1. (*Continued.*)
flowers (F), and rosette leaves (G and H), showing reporter gene expression in the vasculature. Black arrowheads indicate cells with GUS staining, and white arrowheads indicate cells lacking GUS staining. For B, transgenic *ProSNBE:GFP:GUS* seedlings were grown for 20 d in a long-day photoperiod. For C to H, transgenic *ProSNBE:GFP:GUS* plants were grown for 6 weeks in a short-day photoperiod followed by 5 weeks in a long-day photoperiod. If, Interfascicular fibers; Mx, metaxylem; Pi, pith; Px, protoxylem; V, vessel; Xf, xylary fiber.
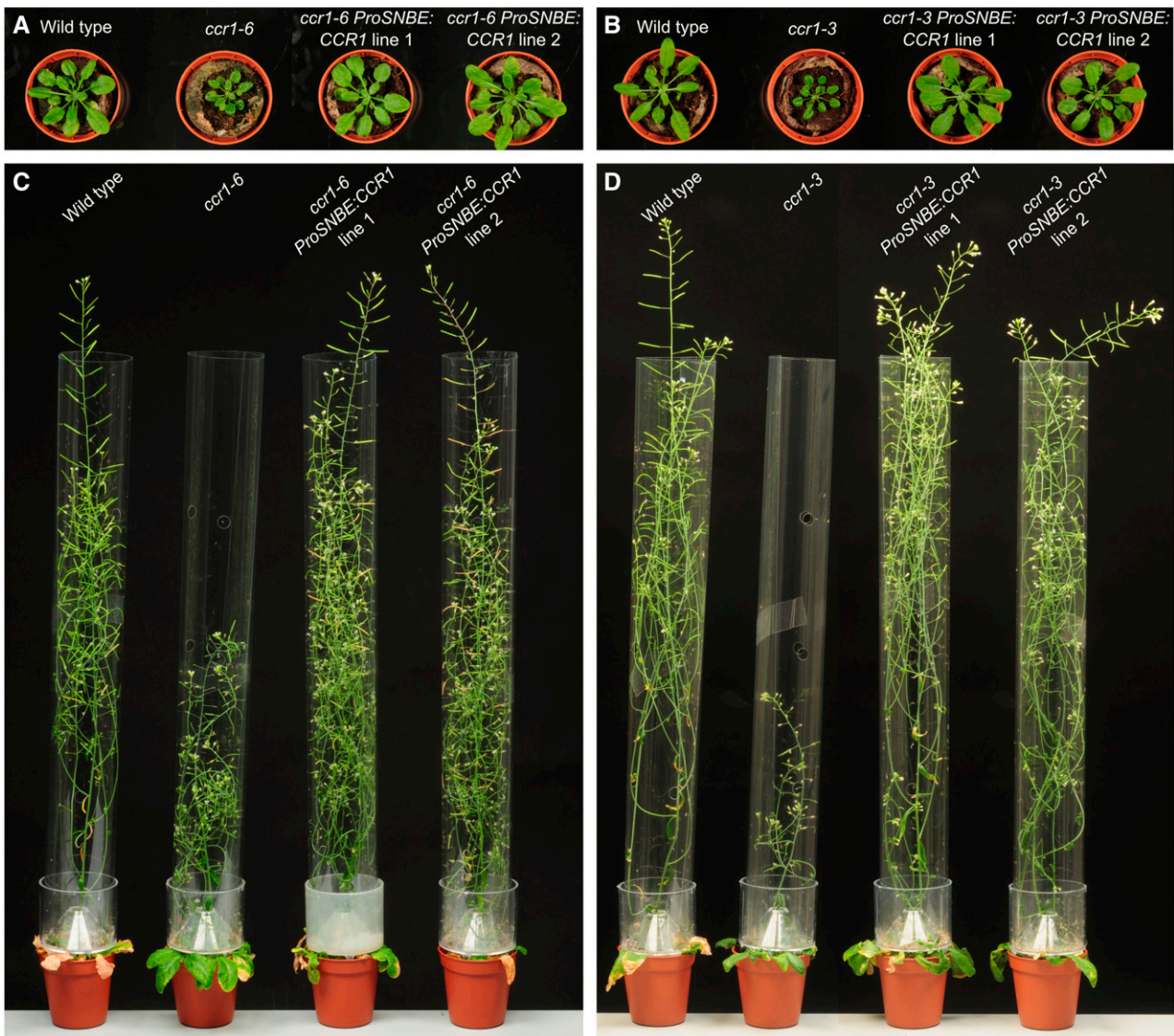
Figure 2. Phenotype of *ccr1 ProSNBE:CCR1* lines. Wild-type, *ccr1*, and *ccr1 ProSNBE:CCR1* plants are shown after cultivation for 6 weeks in a short-day photoperiod followed by 1.5 weeks (A and B) or 5 weeks (C and D) in a long-day photoperiod.

fiber cells of the wild type were devoid of cellular content, whereas those of the *ccr1-6* and *ccr1-6 ProSNBE:CCR1* lines still contained cellular contents. These results indicated that *ccr1-6* and *ccr1-6 ProSNBE:CCR1* did not complete programmed cell death at the time of harvest, despite the fact that all the lines were harvested at the same age.

Based on the lignin and cell wall visualization methods, the xylem of the wild type and *ccr1 ProSNBE:CCR1* lines appeared to be similar (Figs. 3 and 4; Supplemental Fig. S2). Additionally, both the vessels and xylary fibers of *ccr1 ProSNBE:CCR1* seemed to be lignified (Fig. 3; Supplemental Fig. S2). To investigate lignin amount and composition in the different cell types, Raman microscopy analysis was performed (Fig. 5; Supplemental Fig. S3). First, the distribution of components having aromatic ring structures (i.e. building

blocks of the lignin polymer) was visualized by integrating the intensity of each spectrum in the range of 1,650 to 1,550 cm^{-1} into 2D mappings. In the xylem, the intensity of the aromatic ring stretching was high in the wild type, intermediate in the *ccr1-6 ProSNBE:CCR1* lines, and low in *ccr1-6*. In the interfascicular region, the mappings of *ccr1-6* and *ccr1-6 ProSNBE:CCR1* lines showed a similar intensity, which was considerably lower compared with that of the wild type. In the next step, a more detailed analysis was performed on the aromatic region of lignin (1,700–1,550 cm^{-1}) obtained from vessels, xylary fibers, and interfascicular fibers. In vessels and xylary fibers, *ccr1-6* mutants showed a drastic decrease in the aromatic stretching vibration of lignin at 1,597 cm^{-1} (Agarwal et al., 1997) when compared with the wild type, whereas the *ccr1-6 ProSNBE:CCR1* lines had band intensities between those of the

Table I. *Biomass measurements of ccr1 ProSNBE:CCR1 lines*

Measurements were performed on fully senesced plants. For the stem measurements, the leaves, siliques, and seeds were removed. The data represent average values ± SD and the number of repeats are indicated by asterisks: *, 20 repeats for the wild type and the *ccr1 ProSNBE:CCR1* lines and 40 repeats for the *ccr1* mutants; **, 12 repeats for the wild type and the *ccr1 ProSNBE:CCR1* lines and 24 repeats for the *ccr1* mutants; and ***, six repeats for the wild type and the *ccr1 ProSNBE:CCR1* lines and 12 repeats for the *ccr1* mutants. Note that the set containing *ccr1-3, ccr1-3 ProSNBE:CCR1*, and wild-type plants and the set containing *ccr1-6, ccr1-6 ProSNBE:CCR1*, and wild-type plants were grown in two independent experiments. Different letters represent significant differences at the 0.05 significance level (Dunnett-Hsu adjusted Student's *t* test). Total plant biomass = biomass of the aerial part of the plant, just above the rosette.

Line	Primary Inflorescence Stem Height* (cm)	Primary Inflorescence Stem Mass* (mg)	No. Originating from Rosette**	Secondary Inflorescence Stems No. Originating from Primary Inflorescence Stem**	Secondary Inflorescence Stems Total**	Secondary Inflorescence Stems Mass** (mg)	Seeds No.***	Seeds Mass per Seed*** (µg)	Seeds Total Mass* (mg)	Total Stem Biomass** (mg)	Total Plant Biomass* (mg)
Wild type	49.9 ± 4.9 a	43.4 ± 10.5 a	2.6 ± 1.0 a	6.2 ± 0.9 a	8.8 ± 1.2 a	213 ± 30 a	9,343 ± 1,002 a	27.3 ± 1.5 a	266 ± 48 a	262 ± 41 a	765 ± 124 a
ccr1-3	29.3 ± 3.9 b	23.0 ± 5.4 b	3.1 ± 1.2 a	4.8 ± 1.1 b	7.9 ± 1.8 a	108 ± 26 b	898 ± 431 b	34.8 ± 1.8 b	29 ± 15 b	143 ± 38 b	288 ± 92 b
ccr1-3 ProSNBECCR1 line 1	51.3 ± 4.6 a	51.5 ± 6.0 c	5.7 ± 1.0 b	6.5 ± 1.1 a	12.1 ± 1.7 b	373 ± 67 c	5,110 ± 944 c	31.5 ± 1.0 c	157 ± 58 c	416 ± 70 c	844 ± 113 c
ccr1-3 ProSNBECCR1 line 2	51.0 ± 3.8 a	47.1 ± 7.6 a,c	5.3 ± 1.8 b	5.7 ± 0.8 a	11.0 ± 2.0 b	318 ± 75 d	4,409 ± 1,221 c	30.8 ± 1.7 c	134 ± 46 c	373 ± 91 c	780 ± 79 a,c
Wild type	48.2 ± 3.1 a	44.0 ± 10.0 a	1.6 ± 1.1 a	6.1 ± 0.9 a,b	7.7 ± 1.4 a	116 ± 39 a	8,373 ± 2,390 a	26.8 ± 2.5 a	189 ± 71 a	155 ± 46 a	522 ± 154 a
ccr1-6	24.9 ± 2.5 b	24.8 ± 4.6 b	4.4 ± 1.1 b	5.4 ± 0.9 a	9.8 ± 1.3 b	96 ± 27a	1,513 ± 469 b	33.6 ± 2.2 b	45 ± 24 b	120 ± 30 b	265 ± 73 b
ccr1-6 ProSNBECCR1 line 1	50.2 ± 4.2 a	48.2 ± 9.6 a	4.5 ± 1.7 b	6.5 ± 0.9 b	11.0 ± 1.4 c	187 ± 50 b	4,023 ± 892 c	32.8 ± 1.3 b	141 ± 32 c	229 ± 46 c	639 ± 113 c
ccr1-6 ProSNBECCR1 line 2	48.7 ± 3.3 a	44.1 ± 9.8 a	4.1 ± 1.9 b	6.6 ± 1.2 b	10.6 ± 1.6 b,c	176 ± 38 b	3,606 ± 1,062 c	32.2 ± 3.1 b	123 ± 38 c	214 ± 40 c	590 ± 192 a,c

wild type and *ccr1-6*. First, these results indicated that the lignin levels in the vessels of *ccr1-6 SNBE:CCR1* were not recovered to wild-type levels but, rather, were intermediate between the high levels found in the wild type and the drastically reduced levels in *ccr1-6*. Second, we could conclude that the lignin content in the xylary fibers of *ccr1-6 ProSNBE:CCR1* lines also was partially recovered to levels between those of the wild type and *ccr1-6*. In accordance with the lignin staining data, the lignin content in interfascicular fibers (based on peak intensities for the lignin aromatic stretching at 1,597 cm^{-1}) of *ccr1-6* and *ccr1-6 ProSNBE:CCR1* lines was reduced drastically when compared with the wild type. Another difference was observed for the peak at 1,657 cm^{-1}, which is assigned mainly to coniferyl alcohol (C=C stretching of coniferyl alcohol and C=O stretching of coniferaldehyde; Agarwal et al., 2011). Whereas the wild type showed a high intensity for this peak in vessels, xylary fibers, and interfascicular fibers, it was absent in all regions of *ccr1-6*. In the vessels and xylary fibers of *ccr1-6 ProSNBE:CCR1* lines, the intensity of the peak at 1,657 cm^{-1} was intermediate between that of the wild type and *ccr1-6*, whereas in *ccr1-6 ProSNBE:CCR1* interfascicular fibers, the peak at 1,657 cm^{-1} was absent. Interestingly, in vessels and fibers of *ccr1-6*, a new band appeared at 1,633 cm^{-1}. This band was also present in the interfascicular region of *ccr1-6 ProSNBE:CCR1* lines and is known as C=C stretching of ferulic acid (Agarwal and Atalla, 1990; Prinsloo et al., 2004; Meyer et al., 2011; Mateu et al., 2016).

Finally, the stiffness of the stems was determined via a two-point bending test (Supplemental Table S2). Whereas wild-type stems had a bending modulus of 112.5 kPa, *ccr1-6 ProSNBE:CCR1* lines 1 and 2 had significantly reduced bending moduli of 49.4 and 60.2 kPa, respectively. Similarly, the bending modulus of *ccr1-6* also was reduced significantly when compared with the wild type, to a value of 25.7 kPa. Based on this, we could conclude that the stiffness of the stems of *ccr1-6 ProSNBE:CCR1* lines was partially restored when compared with that of *ccr1-6* but was still decreased when compared with that of the wild type.

The Metabolism of *ccr1-6 ProSNBE:CCR1* Lines Shows Characteristics of *ccr1-6* Mutants and of Wild-Type Plants

The biomass penalty and vessel collapse provoked by the *ccr1* mutation were recovered in *ccr1 ProSNBE:CCR1* lines (Table I; Fig. 3; Supplemental Fig. S2). To examine whether the molecular phenotype of *ccr1* mutants was also recovered for *ccr1 ProSNBE:CCR1* lines, metabolic profiling of their inflorescence stems was performed via ultra-high-pressure liquid chromatography-mass spectrometry (UHPLC-MS). This procedure allows the detection of several classes of phenolic compounds and glucosinolates (Vanholme et al., 2012, 2013b; Sundin et al., 2014). A total of 9,746 peaks (mass-to-charge ratio [*m/z*] features) were integrated in the chromatograms of the wild

De Meester et al.

Table II. *Stem biomass measurements of ccr1-6 ProSNBE:CCR1 lines of which developing siliques were repeatedly removed during plant growth*

Measurements were performed on fully senesced plants grown without (control) or with the removal of siliques. The data represent average values ± SD of 12 repeats for the wild type and the ccr1-6 ProSNBE:CCR1 lines and 18 repeats for the ccr1-6 mutants. Statistical analysis focused on the differences between the lines within a treatment (control or with siliques removed). Different letters represent significant differences within a treatment at the 0.05 significance level (Dunnett-Hsu adjusted Student's t test).

Line	Control				With Siliques Removed			
	Secondary Inflorescence Stems				Secondary Inflorescence Stems			
	No. Originating from Rosette	No. Originating from Primary Inflorescence Stem	Total	Total Stem Biomass	No. Originating from Rosette	No. Originating from Primary Inflorescence Stem	Total	Total Stem Biomass
				mg				*mg*
Wild type	2.3 ± 1.0 a	6.1 ± 1.2 a,b	8.4 ± 0.5 a	192.1 ± 47.7 a	5.4 ± 1.5 a,b	7.8 ± 1.1 a	13.3 ± 1.4 a,b	480.9 ± 111.7 a
ccr1-6	3.7 ± 0.6 b	5.1 ± 0.8 a	8.8 ± 1.1 a	122.3 ± 45.3 a	4.5 ± 1.6 a	7.2 ± 1.6 a	11.7 ± 1.9 a	190.3 ± 62.0 b
ccr1-6 ProSNBE:CCR1 line 1	4.8 ± 1.4 b	6.6 ± 1.1 b	11.4 ± 2.1 b	335.6 ± 102.8 b	6.0 ± 1.7 b	7.9 ± 2.0 a	13.9 ± 2.6 b	535.1 ± 103.3 a
ccr1-6 ProSNBE:CCR1 line 2	4.5 ± 1.3 b	6.4 ± 0.7 b	10.9 ± 1.6 b	350.4 ± 74.5 b	5.8 ± 1.3 a,b	8.4 ± 1.0 a	14.2 ± 1.5 b	479.6 ± 58.7 a

type, *ccr1-6*, and *ccr1-6 ProSNBE:CCR1* lines 1 and 2 (Supplemental Data Set S1). After applying stringent filters, 554 peaks were retained for statistical analysis (see "Materials and Methods"). Principal component analysis (PCA) of these 554 peaks showed that the metabolic profiles of *ccr1-6 ProSNBE:CCR1* plants were situated between those of *ccr1-6* mutants and wild-type plants according to the first principal component, which explains 33.5% of the variation (Fig. 6). The second principal component, which explains 15.4% of the variation, reflects variation within the genotypes (and not between the genotypes) and can be attributed to biological and/or technical variation. One-way ANOVA followed by posthoc Student's t tests resulted in a list of 232 peaks with significantly different intensities between the *ccr1-6 ProSNBE:CCR1* lines and the wild type and/or the *ccr1-6 ProSNBE:CCR1* lines and *ccr1-6*. Based on this, the peaks were classified into eight different groups (Fig. 6; Supplemental Data Set S1). Because no significant differences in peak intensity were found between *ccr1-6 ProSNBE:CCR1* lines 1 and 2 for these 232 peaks, the two *ccr1-6 ProSNBE:CCR1* lines were treated further as one line. In-depth analysis of the 232 peaks showed that these could be assigned to 172 compounds, of which 82 could be putatively structurally characterized based on their *m/z*, retention times, and tandem mass spectrometry (MS/MS) fragmentation spectra (Fig. 7; Supplemental Tables S3 and S4; Supplemental Fig. S4). The latter were biochemically classified and situated onto a metabolic map of the phenolic and glucosinolate metabolism in Arabidopsis stems (Fig. 8).

Of the 82 putatively structurally characterized metabolites, 52 belonged to the classes of ferulic acid, vanillic acid, sinapic acid, and syringic acid coupling products and derivatives. Previously, *ccr1* mutants have been described to accumulate members of these metabolic classes (Vanholme et al., 2012). The abundances of these metabolites also were higher in *ccr1-6 ProSNBE:CCR1* when compared with the wild type, of which nine compounds had levels that were even higher than those in *ccr1-6* (group 1), 17 compounds had levels not significantly different from those in *ccr1-6* (group 2), and 26 compounds had levels lower than those in *ccr1-6* (group 3). Furthermore, six compounds were classified as oligolignols and hexosylated oligolignols. The abundance of these metabolic classes was severely reduced in *ccr1-6* mutants when compared with the wild type (Vanholme et al., 2012). In the *ccr1-6 ProSNBE:CCR1* lines, the peak intensities of these metabolites were also reduced when compared with the wild type, to levels higher than in *ccr1-6* (one hexosylated oligolignol in group 6), not significantly different from in *ccr1-6* (two hexosylated oligolignols and two oligolignols in group 7), or lower than in *ccr1-6* (one hexosylated oligolignol in group 8). Another class of phenylpropanoic acid-derived metabolites in Arabidopsis comprises coupling products of monolignols and ferulic acid or sinapic acid. Similar to (hexosylated) oligolignols, the abundance of monolignol-ferulic acid
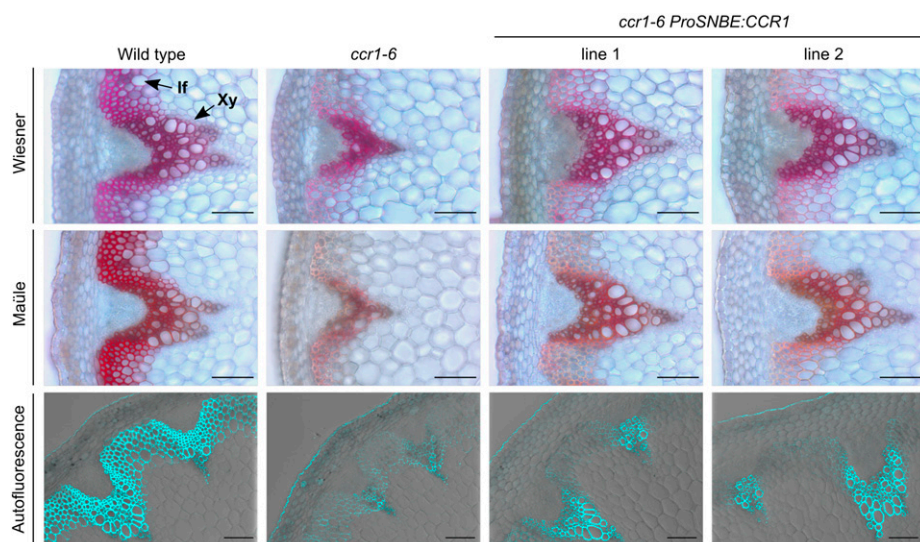
Figure 3. Lignin deposition in inflorescence stems of *ccr1-6 ProSNBE:CCR1* lines. Transverse stem sections are shown for the wild type, *ccr1-6*, and *ccr1-6 ProSNBE:CCR1* lines. Wiesner and Mäule staining and lignin autofluorescence are shown. If, Interfascicular fibers; Xy, xylem. Bars = 100 μm.

coupling products was reduced in *ccr1-6* mutants (Vanholme et al., 2012). In *ccr1-6 ProSNBE:CCR1* lines, the abundance of one monolignol-ferulic acid coupling product was not significantly different when compared with the wild type and increased significantly as compared with *ccr1-6* (group 4). However, the abundance of 14 monolignol-ferulic acid and -sinapic acid coupling products was still reduced in the *ccr1-6 ProSNBE:CCR1* lines as compared with their abundance in the wild type, of which nine had abundances intermediate between those of the wild type and *ccr1-6* (group 6), four had abundances that were not significantly different from those of *ccr1-6* (group 7), and one had an abundance lower than that of *ccr1-6* (group 8). In addition, five glucosinolates that accumulated to high levels in *ccr1-6* were (partially) restored to wild-type levels in *ccr1-6 ProSNBE:CCR1* (groups 3 and 5). Furthermore, the abundances of *N*-acetyl-phenylalanine and *p*-coumaroyl glutamate were decreased in the *ccr1-6* mutant when compared with the wild type, whereas the *ccr1-6 ProSNBE:CCR1* lines had levels intermediate between those of the wild type and *ccr1-6* (group 6). The abundance of *p*-coumaroyl hexose was increased to a similar level in *ccr1-6* and the *ccr1-6 ProSNBE:CCR1* lines when

compared with that of the wild type (group 2). Finally, caffeic acid 3/4-*O*-hexoside accumulated to high levels in *ccr1-6* mutants when compared with the wild type but was reduced again to wild-type levels in the *ccr1-6 ProSNBE:CCR1* lines (group 5). Despite the notable exceptions, we found that the majority of metabolic shifts present in dwarfed *ccr1-6* mutants were still largely present in the phenotypically fully recovered *ccr1 ProSNBE:CCR1* lines.

The Effect of Ferulic Acid Content on Cell Proliferation and Growth

It has been proposed that the dwarfed phenotype of *ccr1* mutants is caused by the dramatically increased level of ferulic acid (Xue et al., 2015). These high levels of ferulic acid were reported to delay the exit from cell proliferation, thereby reducing the average nuclear ploidy level and causing the observed growth defects of *ccr1* mutants (Xue et al., 2015). Elaborating on this reasoning, the ferulic acid levels of the growth-restored *ccr1-6 ProSNBE:CCR1* lines should be reduced when compared with *ccr1-6*, leading to restoration of the cell
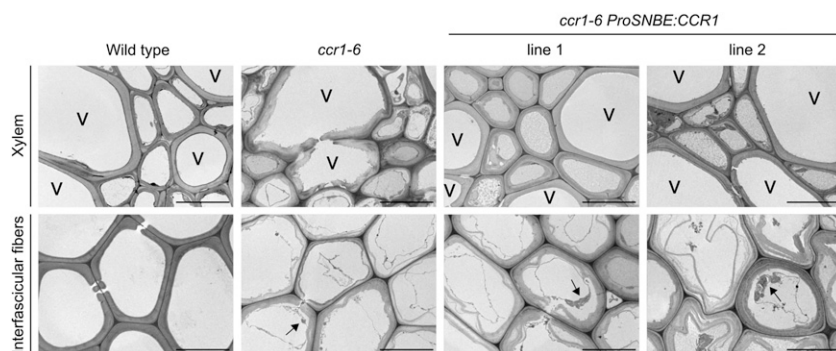
Figure 4. Morphology of cell walls of wild-type, *ccr1-6*, and *ccr1-6 ProSNBE:CCR1* stems. Transmission electron microscopy demonstrates the ultrastructure of the interfascicular fibers and xylem regions. Arrows indicate residual cellular content. V, Xylary vessel. Bars = 10 μm.
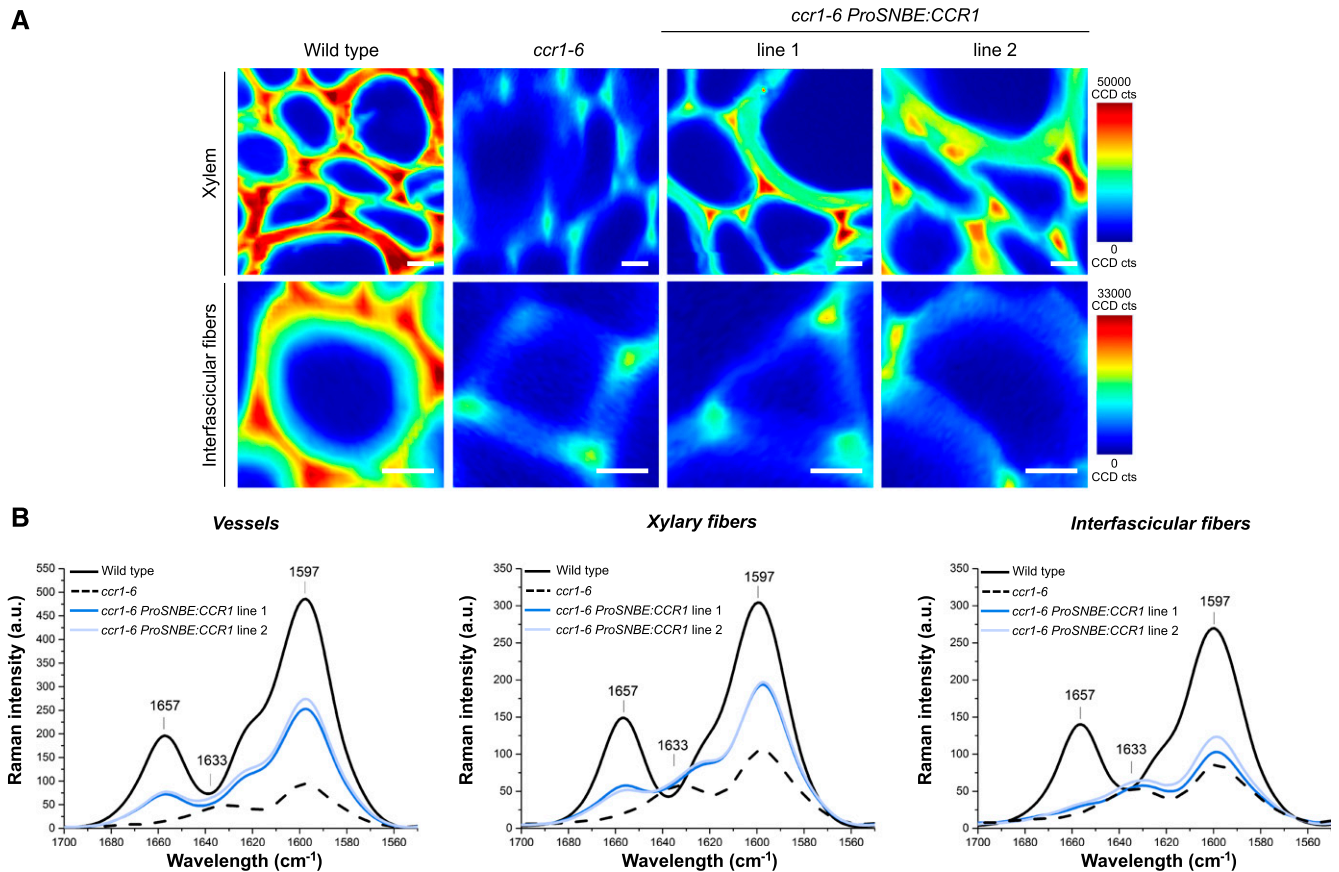
Figure 5. Raman microscopy analysis of cell walls of wild-type, *ccr1-6*, and *ccr1-6 ProSNBE:CCR1* plants. A, Examples of Raman mapping images taken from the xylem and interfascicular fiber region of the wild type, *ccr1-6*, and *ccr1-6 ProSNBE:CCR1* lines by integrating the aromatic stretching vibration from 1,650 to 1,550 cm^{-1}. CCD cts, Charged Coupled Device counts. Bars = 10 μm. B, Extracted average spectra in the lignin aromatic region between 1,700 and 1,550 cm^{-1} obtained by a region-of-interest study in vessels, xylary fibers, and interfascicular fibers (n = 18: 3 biological replicates × 2 mappings × 3 regions of interest). The marked bands represent 1,657 cm^{-1} (C=C stretching of coniferyl alcohol plus C=O stretching of coniferaldehyde), 1,633 cm^{-1} (C=C stretching from the propenoic acid side chain of ferulic acid), and 1,597 cm^{-1} (aromatic ring stretching of lignin). a.u., arbitrary units.

cycle and growth. To test this hypothesis, we determined the ferulic acid levels and nuclear ploidy level of *ccr1-6 ProSNBE:CCR1* lines using the wild type and *ccr1-6* as a control. In analogy with Xue et al. (2015), all experiments were performed on the first pair of leaves of 15- and 25-d-old plants. At both time points, the rosette sizes of *ccr1-6 ProSNBE:CCR1* plants were similar to those of the wild type, whereas *ccr1-6* rosettes were significantly smaller (Supplemental Fig. S5). Additionally, the morphology of the vasculature of the first leaves was investigated via microscopy. Notably, wild-type and *ccr1-6 ProSNBE:CCR1* plants had large and open vessels in the xylem, whereas the vessels of *ccr1-6* mutants were collapsed (Supplemental Fig. S6).

In contrast to the findings of Xue et al. (2015), the levels of ferulic acid remained below the detection limit in all samples in our analysis. Therefore, a series of ferulic acid coupling products was used as a measure for the total ferulic acid content (Table III). On day 15, the levels of all ferulic acid coupling products were

increased in *ccr1-6 ProSNBE:CCR1* lines when compared with the wild type, to levels equal to those in the *ccr1-6* mutant (Table III). The same trend was observed for seedlings on day 25. At this time point, the levels of ferulic acid coupling products were increased in the *ccr1-6 ProSNBE:CCR1* lines when compared with the wild type, to levels equal to or lower than in the *ccr1-6* mutant (Table III). In accordance with the literature, the average nuclear ploidy level of cells from *ccr1-6* mutants was lower as compared with that of the wild type at both time points (Fig. 9; Xue et al., 2015). However, the average ploidy level of cells in both *ccr1-6 ProSNBE:CCR1* lines was similar to that of the wild type and significantly higher than that of the *ccr1-6* mutant at both time points (Fig. 9). Taken together, these results show that the overall level of ferulic acid was similar in both *ccr1-6* and *ccr1-6 ProSNBE:CCR1* seedlings, whereas cells of the *ccr1-6* mutant, but not those of *ccr1-6 ProSNBE:CCR1*, retained their mitotic state for a prolonged time.

A
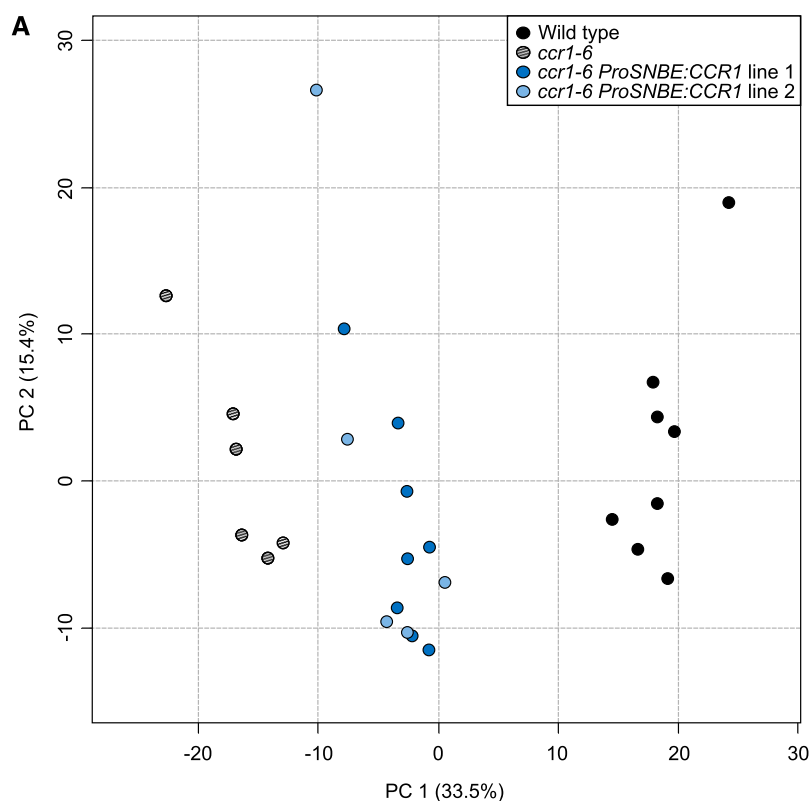
Figure 6. Summary of metabolite profiling of primary inflorescence stems of the wild type, *ccr1-6*, and *ccr1-6 ProSNBE:CCR1*. A total of 9,746 peaks were detected over the different samples (wild type, *n* = 8; *ccr1-6*, *n* = 6; and *ccr1-6 ProSNBE:CCR1*, *n* = 13). After applying stringent filters, 554 peaks were selected for PCA and statistical analysis. A, PCA of the selected peaks revealed that the first principal component (PC 1; 33.5% of variation) explained mainly the difference between genotypes. The second principal component (PC 2; 15.4% of the variation) reflects the variation within the genotypes. B, Further statistical analysis revealed that the peak intensities of 232 compounds were significantly different in *ccr1-6 ProSNBE:CCR1* when compared with the wild type and when compared with *ccr1-6*. The differentially accumulating metabolites were classified into eight groups. Per group, the number of peaks, corresponding compounds, and annotated compounds are given.

B

Group	Compound abundance in *ccr1-6 ProSNBE:CCR1* compared to wild type	Compound abundance in *ccr1-6 ProSNBE:CCR1* compared to *ccr1-6*	Number of peaks	Number of compounds	Number of annotated compounds
1	Increased	Increased	27	23	9
2	Increased	Not differential	69	37	18
3	Increased	Decreased	62	51	29
4	Not differential	Increased	9	7	1
5	Not differential	Decreased	6	6	3
6	Decreased	Increased	29	24	12
7	Decreased	Not differential	26	20	8
8	Decreased	Decreased	4	4	2

The Lignocellulosic Composition of *ccr1 ProSNBE:CCR1* Is Highly Similar to That of the *ccr1* Mutant

Lignocellulosic biomass is recalcitrant toward deconstruction mainly because of the presence of lignin. Because *ccr1 ProSNBE:CCR1* lines do not suffer from a yield penalty but have a reduced amount of lignin in both the xylem and interfascicular fibers (Fig. 5), translation of this strategy in a bioenergy crop could be interesting for the biorefinery. To study the lignocellulosic biomass composition of *ccr1-6 ProSNBE:CCR1*, the lignin content and composition and cellulose content of senesced inflorescence stems were determined (Table IV). First, soluble compounds were removed from the stems by applying a sequential extraction to produce CWR (Van Acker et al., 2013). In compliance with the

literature, *ccr1-6* mutants had 12% less CWR, and thus relatively more soluble compounds, than the wild type (Van Acker et al., 2013). On average, the *ccr1-6 ProSNBE:CCR1* lines had 6% less CWR than the wild type. Second, the fraction of lignin in these prepared CWRs was determined via the Klason method. The lignin amount of the *ccr1-6 ProSNBE:CCR1* lines did not differ significantly from that of *ccr1-6* but was approximately half that of the wild type. Third, the lignin composition was analyzed via thioacidolysis, which allows quantification of the H, G, S, and other minor units that are linked by β-O-4 interunit bonds in the lignin polymer. Lignins from both the *ccr1-6* and *ccr1-6 ProSNBE:CCR1* lines released substantially fewer monomers (H + G + S) than the lignin from wild-type

Figure 7 — List of putatively structurally characterized metabolites with a different abundance in inflorescence stems

average peak intensity columns: Wild type | ccr1-6 | ccr1-6 ProSNBE:CCR1

vanillic acid and ferulic acid coupling products and derivatives

no.	name
1.1	ferulic acid 4-O-hexoside 1
1.2	feruloyl hexose 4-O-hexoside
1.3	feruloyl hexose + sulfate
1.4	ferulic acid + hexose + sulfate
1.5	vanillic acid + ferulic acid + hexose + hexose 1
1.6	vanillic acid + ferulic acid + hexose + hexose + hexose 1
2.1	feruloyl hexose 1
2.2	feruloyl hexose 2
2.3	feruloyl malate 1
2.4	feruloyl malate 2
2.5	feruloyl glutamate 1
2.6	ferulic acid + sulfate
2.7	ferulic acid + malate + sulfate
2.8	dihydroferulic acid + hexose
2.9	5-hydroxyferulic acid + hexose 1
2.10	5-hydroxyferulic acid + malate
2.11	vanilloyl hexose
2.12	vanillic acid + dihydrocaffeic acid + hexose + hexose
2.13	vanillic acid + ferulic acid + hexose + hexose + hexose 2
3.1	ferulic acid 4-O-hexoside 2
3.2	feruloyl glutamate 2
3.3	ferulic acid + malate + deoxyhexose 1
3.4	ferulic acid + malate + deoxyhexose 2
3.5	5-hydroxyferulic acid + hexose 2
3.6	vanillic acid 4-O-hexoside
3.7	vanilloyl malate
3.8	vanilloyl malate 4-O-hexoside
3.9	vanillic acid + vanillic acid + hexose
3.10	vanillic acid + vanillic acid + hexose + hexose
3.11	vanillic acid + vanillic acid + hexose + hexose + hexose 1
3.12	vanillic acid + vanillic acid + hexose + hexose + hexose 2
3.13	vanillic acid + vanillic acid + vanillic acid + hexose + hexose
3.14	vanillic acid + acetovanillone + hexose + hexose
3.15	acetovanillone 4-O-hexoside
3.16	hydroxyvanillic acid + hexose
3.17	vanillic acid + dihydroferulic acid + hexose
3.18	vanillic acid + ferulic acid + hexose + hexose 2
3.19	vanillic acid + dihydroferulic acid + hexose + hexose 1
3.20	vanillic acid + dihydroferulic acid + hexose + hexose 2
3.21	vanillic acid + dihydroferulic acid + hexose + hexose + hexose
3.22	vanillic acid + vanillic acid + dihydroferulic acid + hexose + hexose + hexose

sinapic acid and syringic acid coupling products

no.	name
1.7	sinapic acid 4-O-hexoside
1.8	sinapoyl hexose
1.9	disinapoyl hexose
2.14	sinapoyl malate 1
2.15	sinapoyl malate 2
2.16	sinapoyl glutamate
2.17	syringoyl hexose
3.23	syringic acid 4-O-hexoside

ferulic acid, vanillic acid, sinapic acid and syringic acid coupling products and derivatives

no.	name
3.24	dihydroferulic acid + syringic acid + hexose + hexose
3.25	vanillic acid + syringic acid + hexose + hexose 1
3.26	vanillic acid + syringic acid + hexose + hexose 2

monolignol-ferulic acid coupling products

no.	name
4.1	G(8-5)ferulic acid + malate + hexose
6.1	G(8-O-4)feruloyl hexose 1
6.2	G(8-O-4)feruloyl hexose 2
6.3	G(8-O-4)feruloyl hexose 3
6.4	G(8-O-4)feruloyl hexose 4
6.5	G(8-O-4)ferulic acid + hexose
6.6	G(8-O-4)feruloyl malate
6.7	G(8-O-4)ferulic acid + malate 1
6.8	G(8-O-4)ferulic acid + malate 2
6.9	G(8-O-4)ferulic acid + hexose + malate
7.1	S(8-O-4)ferulic acid + malate
7.2	G(8-5)feruloyl malate
7.3	G(8-O-4)S(8-5)ferulic acid + malate
8.1	G(8-O-4)ferulic acid + vanillic acid + hexose

monolignol-sinapic acid coupling products

no.	name
7.4	G(8-O-4)sinapic acid + malate

oligolignols

no.	name
7.5	G(8-O-4)S(8-5)G
7.6	G(8-O-4)S(8-5)G'

hexosylated oligolignols

no.	name
6.10	G(8-8)G 4-O-dihexoside
7.7	G(red8-5)G + hexose
7.8	G(8-O-4)S/G(8-8)G/S hexoside
8.2	G-4-O-hexoside(8-O-4)S

indolic glucosinolates

no.	name
3.27	4-hydroxyglucobrassicin
3.28	5'-O-β-D glucosyl dihydroascorbigen
5.1	neoglucobrassicin
5.2	dihydroxyglucobrassicin

methylalkyl glucosinolates

no.	name
3.29	2-hydroxypentyl glucosinolate

others

no.	name
2.18	p-coumaroyl hexose
5.3	caffeic acid 3/4-O-hexoside
6.11	p-coumaroyl glutamate
6.12	N-acetylphenylalanine

Figure 7. List of putatively structurally characterized metabolites with a different abundance in inflorescence stems of *ccr1-6 ProSNBE:CCR1* plants as compared with the wild type or *ccr1-6* mutants. Eighty-two compounds were characterized, of which the abundance was significantly different between *ccr1-6 ProSNBE:CCR1* and the wild type, on the one hand, and/or *ccr1-6 ProSNBE:CCR1* and *ccr1-6*, on the other hand. The differentially accumulating metabolites were classified into eight different groups (Fig. 6B). Each putatively structurally characterized metabolite has a unique number that represents (1) the group that the metabolite belongs to and (2) the ranking within this group. The metabolites are listed per metabolic class, and the dashed lines separate the different groups present in a specific metabolic class. The average peak intensities are represented by a heat map, ranging from low values represented in blue to high values represented in red (wild type, n = 8; ccr1-6, n = 6; and ccr1-6 ProSNBE: CCR1, n = 13).

samples. This indicates that the lignins of the *ccr1-6* and *ccr1-6 ProSNBE:CCR1* lines have fewer β-*O*-4 interunit bonds and, thus, are enriched in carbon-carbon (mainly β-5 and β-β) interunit bonds. The H monomers were barely detectable in the wild type and constituted only 1.8% of the total identified thioacidolysis-released units. By contrast, the *ccr1-6* and *ccr1-6 ProSNBE:CCR1* lines showed a relative increase in thioacidolysis-released H units by approximately 3-fold. Furthermore, the S/G ratio was decreased for the *ccr1-6* mutant when compared with that of the wild type. Interestingly, this decrease was even more strikingly pronounced for the *ccr1-6 ProSNBE:CCR1* lines. Incorporation of ferulic acid (FA), which is a known minor constituent of lignin, results in the release of three different units after thioacidolysis: two are linked via conventional β-*O*-4 structures (the β-*O*-4-FA-I and β-*O*-4-FA-II units), while the third, derived from the bis-β-*O*-4 coupling of ferulic acid, results in a truncated side chain (Ralph et al., 2008). In agreement with previously reported results for plants deficient in CCR, the relative abundance of all three ferulic acid units was increased in the *ccr1-6* mutant when compared with the levels in the wild type (Goujon et al., 2003; Leplé et al., 2007; Mir Derikvand et al., 2008; Ralph et al., 2008; Van Acker et al., 2014). Interestingly, the *ccr1-6 ProSNBE:CCR1* lines also showed a relative increase in all three thioacidolysis-released ferulic acid units when compared with the wild type, to levels not significantly different from those in the *ccr1-6* mutant. Fourth, crystalline cellulose content was analyzed via the spectrophotometric phenol-sulfuric acid assay. In accordance with previously published results (Van Acker et al., 2013), *ccr1-6* mutants had less crystalline cellulose than the wild type (with an average relative decrease of about 17%). The crystalline cellulose content in the *ccr1-6 ProSNBE:CCR1* lines did not differ significantly from that of the *ccr1-6* mutants but was reduced as compared with that of the wild type.

The *ccr1 ProSNBE:CCR1* Lines Have a 4-Fold Increase in Total Plant Saccharification Yield When Compared with the Wild Type

Cell wall analysis revealed that the lignin content of the *ccr1-6 ProSNBE:CCR1* lines was reduced when compared with that of the wild type, to levels similar to those of the *ccr1-6* mutant (Table IV). Because the lignin amount has a negative effect on the saccharification efficiency, the saccharification potential of *ccr1-6 ProSNBE:CCR1* biomass after acid, alkaline, or no pretreatment was investigated further. Pretreatment (with acid or alkali) allowed the samples to reach the plateau much sooner (i.e. after 48 h instead of 96 h compared with no pretreatment; Supplemental Fig. S7). Cellulose-to-glucose conversion for the *ccr1-6 ProSNBE:CCR1* lines was similar to that of the *ccr1-6* lines and much higher than that of the wild type, independent of the pretreatment (Fig. 10; Supplemental Fig. S7; Supplemental Table S5). More specifically, the

cellulose-to-glucose conversion of the unpretreated samples had increased from 18% in the wild type to, on average, 65% in the *ccr1-6* and *ccr1-6 ProSNBE:CCR1* lines (i.e. a relative increase of 261%). In the case of acid pretreatment, the conversion increased from 22% in the wild type to, on average, 81% in the *ccr1-6* and *ccr1-6 ProSNBE:CCR1* lines (i.e. a relative increase of 268%). Finally, in the case of alkaline pretreatment, the conversion increased from 17% in the wild type to, on average, 70% in the *ccr1-6* and *ccr1-6 ProSNBE:CCR1* lines (i.e. a relative increase of 312%).

The glucose yield after saccharification was also expressed per plant (i.e. total stem biomass; Fig. 10). In the case of the dwarfed *ccr1-6* mutants, the total glucose release per plant was increased by about 2-fold in comparison with the wild type for each of the tested pretreatments. Due to the combined effect of the increase in total inflorescence stem biomass and the increase in saccharification efficiency, the *ccr1-6 ProSNBE:CCR1* plants showed more than a 4-fold increase in glucose yield per plant when compared with the wild type in each of the tested pretreatments.

DISCUSSION

Vessels Act as Good Neighbors to Xylary Fibers

Complementing *ccr1* mutants with *ProSNBE:CCR1* resulted in plants with restored vessel integrity and growth. Using light, fluorescence, Raman, and electron microscopy, we analyzed the organization of the cell wall and lignin deposition in vessels and (xylary and interfascicular) fibers. Interestingly, lignification in *ccr1 ProSNBE:CCR1* lines was not only (partially) restored in the vessels, but the cell walls of the xylary fibers also showed increased lignification and restored cell wall integrity. The latter is in apparent contrast to the vessel-specific expression pattern conferred by *ProSNBE* (McCarthy et al., 2011; this study). This observation demonstrates that monolignols synthesized in the vessel cells not only lignify the vessel cell wall but also contribute to the lignification of the cell walls of neighboring cells. Previous research in Arabidopsis has revealed that nonlignifying parenchyma cells provide monolignols to vessels and xylary fibers during the lignification process, a property that was termed good neighbors (Smith et al., 2013). In addition, xylary fibers also play a role in the lignification of neighboring vessel elements during xylem development (Smith et al., 2017b). These combined observations show that monolignols can be transported between the different xylem cell types.

Raman microscopy analysis showed that the lignin deposition in the xylem cells of *ccr1 ProSNBE:CCR1* lines is increased by approximately 2-fold when compared with that in the *ccr1* background but is not restored to wild-type levels. This observation could be explained by the fact (1) that *ProSNBE* and the native *CCR1* promoter differ in timing and/or strength of

De Meester et al.
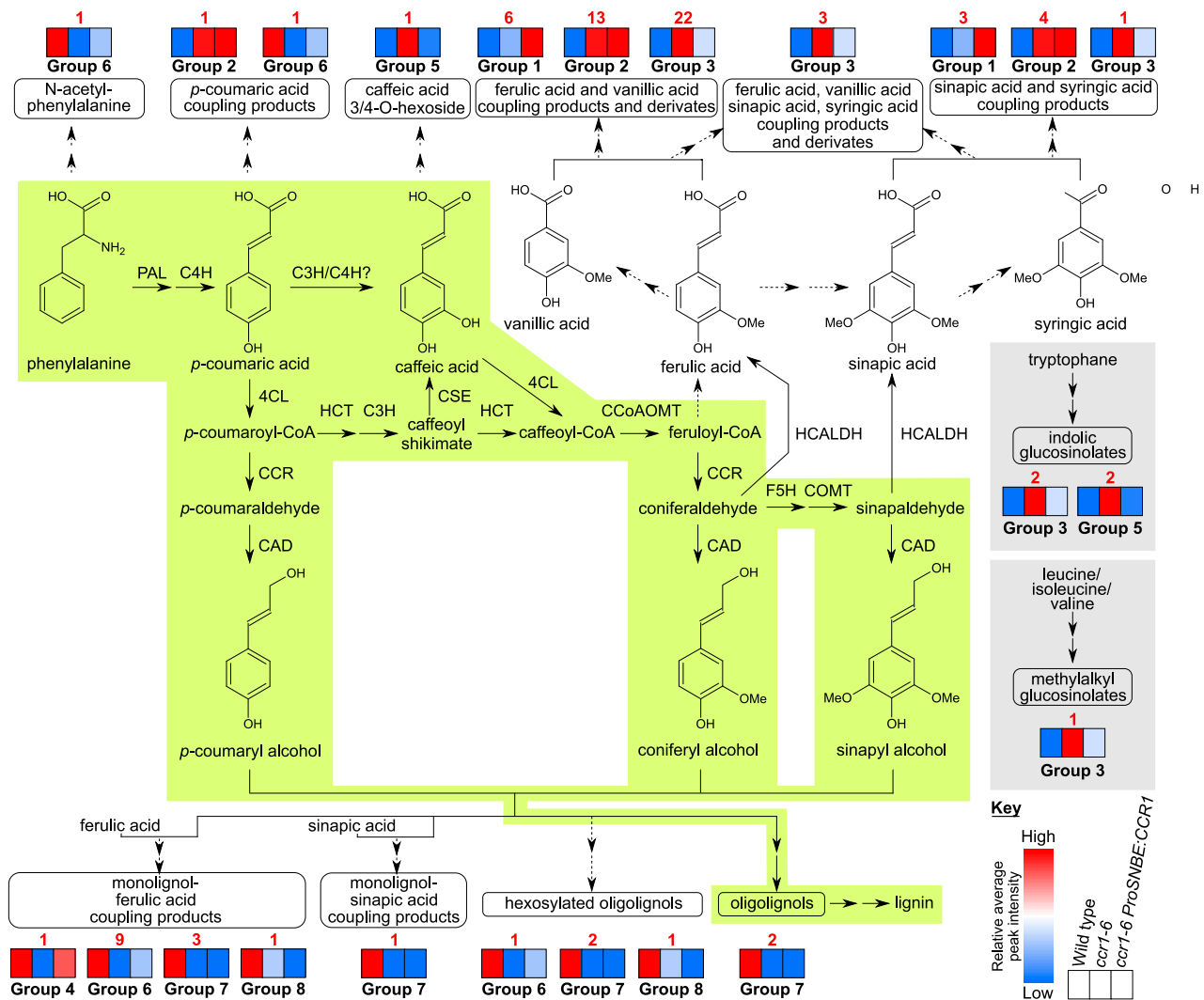
Figure 8. Metabolic map of phenolic and glucosinolate metabolism in the primary inflorescence stems of the wild type, *ccr1-6*, and *ccr1-6 ProSNBE:CCR1* lines. The green highlighted part of the pathway is considered to be the major route for lignin biosynthesis. The gray highlighted part depicts glucosinolate biosynthesis. Dashed arrows represent suggested pathways. Metabolites were classified into one of eight specific groups, based on their abundance in the wild type, *ccr1-6*, and *ccr1-6 ProSNBE:CCR1* (Figs. 6B and 7; Supplemental Table S3). In each group, different metabolite classes are represented (Fig. 7). In the pathway, these different metabolite classes are indicated by round-angled boxes. Per metabolite class, the respective group(s) containing this specific class is (are) indicated, accompanied by heat maps. These heat maps represent the average peak intensities of all characterized metabolites belonging to a specific group for the wild type (first block), *ccr1-6* (second block), and *ccr1-6 ProSNBE: CCR1* (third block), indicated by a range from blue (lowest values) to red (highest values; see key at bottom). The red number indicates the number of metabolites belonging to this group in a specific metabolic class. Terms not defined in the text are as follows: F5H, FERULATE 5-HYDROXYLASE; COMT, CAFFEIC ACID O-METHYLTRANSFERASE; CAD, CINNAMYL ALCOHOL DEHYDROGENASE; HCALH, HYDROXYCINNAMALDEHYDE DEHYDROGENASE (Vanholme et al., 2012; Vanholme et al., 2013b). C3H/C4H?: Interaction between C3H and C4H has been shown for both Arabidopsis and poplar, but activity of the C3H/C4H heterodimer for the conversion of *p*-coumaric acid to caffeic acid has only been shown for poplar (Bassard et al., 2012; Chen et al., 2011).

expression in the vessel cells or (2) that the expression of *CCR1* in the vessels alone is insufficient to compensate for the lack of monolignols that otherwise originate from the vessels, xylary fibers, and parenchyma cells (Smith et al., 2013, 2017b). (3) Furthermore, vessels have been shown to continue lignification following programmed cell death by the donation of monolignols from neighboring parenchyma cells and xylary fibers (Pesquet et al., 2013; Serk et al., 2015; Smith et al., 2017b). Because *CCR1* expression is restored only in the vessels of *ccr1 ProSNBE:CCR1* lines, postmortem lignification is unlikely. Nevertheless, the partial restoration

Table III. *Analysis of ferulic acid content in leaves of 15- and 25-d-old seedlings of the wild type, ccr1-6, and ccr1-6 ProSNBE:CCR1 lines*

The identified ferulic acid coupling products and their average peak area $\pm$ SE are shown (n = 5). Statistics are per compound and per time point (see "Materials and Methods"). Different letters represent significant differences at the 0.01 significance level (Dunnett-Hsu adjusted Student's *t* test). b.d., below detection limit. The asterisk indicates a compound detected as a formic acid adduct.

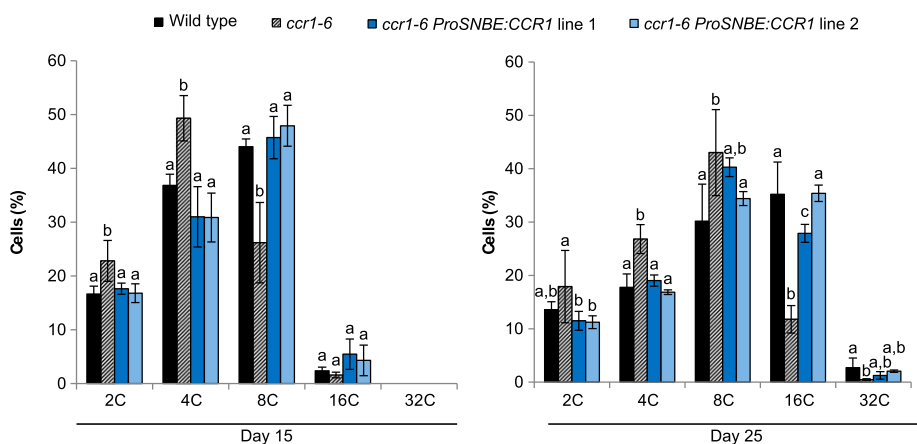| No.	Retention Time	m/z	Compound Name	Day 15			Day 25		
				Wild Type	ccr1-6	ccr1-6 ProSNBE:CCR1	Wild Type	ccr1-6	ccr1-6 ProSNBE:CCR1
	min								
1	3.76	355.103	ferulic acid 4-O-hexoside	3 ± 3 a	282 ± 11 b	272 ± 25 b	5 ± 2 a	258 ± 21 b	169 ± 12 c
2	5.41	355.103	feruloyl hexose	30 ± 27 a	1,178 ± 123 b	1,416 ± 298 b	22 ± 13 a	595 ± 119 b	179 ± 38 c
3	5.52	355.103	ferulic acid + hexose	34 ± 24 a	1,453 ± 98 b	1,553 ± 131 b	85 ± 6 a	1,624 ± 117 b	1,220 ± 75 b
4	8.99	309.060	feruloyl malate	0 ± 0 a	140 ± 10 b	150 ± 14 b	b.d.	b.d.	b.d.
5	6.39	322.093	feruloyl glutamate	11 ± 9 a	1,375 ± 181 b	1,194 ± 172 b	16 ± 3 a	1,007 ± 100 b	321 ± 37 c
6	5.77	322.093	ferulic acid + glutamate	15 ± 11 a	3,119 ± 433 b	3,043 ± 420 b	4 ± 4 a	2,829 ± 272 b	916 ± 132 c
7	2.62	563.161	feruloyl hexose + hexose*	5 ± 5 a	170 ± 22 b	141 ± 25 b	2 ± 2 a	520 ± 65 b	221 ± 44 c
8	5.86	471.114	ferulic acid + malate + hexose	4 ± 3 a	1,335 ± 166 b	795 ± 114 b	7 ± 1 a	1,783 ± 184 b	1,011 ± 109 c
9	8.76	455.118	ferulic acid + malate + deoxyhexose	0 ± 0 a	114 ± 10 b	149 ± 26 b	0 ± 0 a	74 ± 15 b	115 ± 13 b

of lignin deposition in the xylem of *ccr1 ProSNBE:CCR1* appeared to be sufficient for the complete recovery of the stem biomass yield of *ccr1 ProSNBE:CCR1* lines.

Despite Their Phenotypic Recovery, *ccr1-6 ProSNBE:CCR1* Lines Share Many Characteristics with *ccr1-6*

Although being restored in growth, the lignocellulosic composition and metabolome of *ccr1-6 ProSNBE: CCR1* lines were very similar to those of *ccr1-6*. Interestingly, *ccr1-6* and *ccr1-6 ProSNBE:CCR1* also share a similar delay in cell development: whereas the interfascicular fibers of wild-type plants have completed cell death, the interfascicular fibers of *ccr1-6* and *ccr1-6 ProSNBE:CCR1* plants still contain their cellular contents, indicating a delay in programmed cell death. Furthermore, *ccr1-6* mutants had a lower S/G ratio,

which also is characteristic of their delay in lignification and development (Jones et al., 2001; Laskar et al., 2006; Leplé et al., 2007; Ruel et al., 2009). A reduced S/G ratio also was observed for *ccr1-6 ProSNBE:CCR1*, to a level that was even lower than that of *ccr1-6*. The latter also is a consequence of the lignin deposition pattern in *ccr1-6 ProSNBE:CCR1*: because the xylem region is more enriched in G units (while the fibers contain a higher level of S lignin; Pradhan Mitra and Loqué, 2014), (partial) restoration of lignification in the xylem will lead to a further decrease in the S/G ratio in the *ccr1-6 ProSNBE:CCR1* lines.

Additionally, *ccr1-6* mutants have been shown to have a lot of differences in their metabolism when compared with the wild type (Vanholme et al., 2012). These differences could be attributed to their developmental delay and/or the pathway perturbation itself.

Figure 9. Nuclear ploidy levels of wild-type, *ccr1-6*, and *ccr1-6 ProSNBE:CCR1* cells. Flow cytometry analysis is shown for the first leaves at 15 and 25 d post stratification (15 d, n = 4; 25 d, n = 5). Error bars indicate SD. Different letters represent significant differences at the 0.05 significance level (Dunnett-Hsu adjusted Student's *t* test).

Table IV. *Cell wall characteristics*

The cell wall residue (CWR) expressed as a percentage of dry weight was determined gravimetrically after a sequential extraction ($n = 6$). Lignin content was determined with the Klason method and expressed as percentage of CWR ($n = 3$). Lignin composition was determined with thioacidolysis ($n = 6$). The sum of H, G, and S is expressed in $\mu mol\ g^{-1}$ Klason lignin. The relative proportions of the different lignin units were calculated based on the total thioacidolysis yield (including the minor nonconventional lignin units). S/G ratio was calculated based on the absolute values for S and G. β-O-4-FA-I, G-CH=CH-COOH; β-O-4-FA-II, G-CHR-CH$_2$-COOH; bis-β-O-4-FA, G-CHR-CHR$_2$ (R = thioethyl). Cellulose was expressed as a percentage of CWR ($n = 6$). Values given are averages ± sd. Different letters represent significant differences at the 0.05 significance level (Dunnett-Hsu adjusted Student's t test).

Line	CWR	Klason Lignin	Lignin Content and Composition								Crystalline Cellulose
			H + G + S	H	G	S	S/G Ratio	β-O-4-FA-I	β-O-4-FA-II	bis-β-O-4-FA	
	%	% CWR	$\mu mol\ g^{-1}$	%	%	%		%	%	%	% CWR
Wild type	78.5± 1.3 a	18.0± 0.9 a	23.6± 3.5 a	1.8± 0.6 a	71.5± 1.2 a	26.6± 0.9 a	0.37± 0.02 a	0.03± 0.03 a	0.02± 0.00 a	0.09± 0.01 a	44.7± 2.2 a
ccr1-6	69.4± 2.0 b	9.5± 1.0 b	8.9± 1.9 b	5.5± 2.9 b	70.5± 1.5 a	21.9± 3.3 b	0.31± 0.05 b	0.35± 0.25 b	0.40± 0.13 b	1.34± 0.76 b	34.4± 3.2 b
ccr1-6 ProSNBE:CCR1 line 1	74.2± 1.7 c	9.7± 0.5 b	6.9± 1.7 b	5.5± 2.7 b	77.8± 2.6 b	14.2± 1.5 c	0.18± 0.02 c	0.41± 0.26 b	0.46± 0.09 b	1.56± 0.92 b	38.6± 2.5 b
ccr1-6 ProSNBE:CCR1 line 2	73.6± 1.2 c	9.9± 0.3 b	7.4± 1.5 b	5.5± 1.7 b	78.1± 2.7 b	14.0± 2.3 c	0.18± 0.04 c	0.38± 0.17 b	0.54± 0.12 b	1.45± 0.58 b	35.5± 2.3 b

Despite their recovery in growth and partial restoration in *CCR1* expression, *ccr1-6 ProSNBE:CCR1* lines still share most of the shifts in their metabolism with *ccr1-6*. Of the 232 selected peaks, 15 (belonging to groups 4 and 5) were not differential between the wild type and *ccr1-6 ProSNBE:CCR1*, whereas 95 (belonging to groups 2 and 7) were not differential between *ccr1-6* and *ccr1-6 ProSNBE:CCR1*. In addition, both *ccr1-6* and *ccr1-6 ProSNBE:CCR1* accumulate ferulic acid, vanillic acid, sinapic acid, and syringic acid coupling products. Moreover, both lines show a reduction in (hexosylated) oligolignols and monolignol-ferulic acid and -sinapic acid coupling products when compared with the wild type. As a notable exception, glucosinolate levels in *ccr1-6 ProSNBE:CCR1* plants were (partially) restored to wild-type levels. Glucosinolates are involved in plant defense, and their biosynthesis is up-regulated in the case of tissue or cell damage (Del Carmen Martínez-Ballesta et al., 2013). Transcripts of the glucosinolate biosynthesis genes are more abundant in *ccr1* mutants when compared with the wild type (Vanholme et al., 2012). It seems plausible that the accumulation of glucosinolates in *ccr1-6* lines is a consequence of the general stress status of these mutants. Therefore, the lower levels of glucosinolates in *ccr1-6 ProSNBE:CCR1* lines as compared with those in *ccr1-6* could be a reflection of their reduced stress levels caused by the reversal of the *irx* phenotype.

Ferulic Acid Accumulation Is Not the Cause for the Yield Penalty of *ccr1* Mutants

According to Xue et al. (2015), CCR1 plays a dual role in plants: next to being important for lignin biosynthesis, it is required for the termination of cell division. For the latter, CCR1, ferulic acid, and ROS coordinate the cell proliferation exit for leaf development. From day 11 onward, *CCR1* expression covers the entire leaf, resulting into decreased ferulic acid levels in all leaf cells. As ferulic acid antagonizes the effect of ROS, the lower levels of ferulic acid upon *CCR1* expression will lead to an accumulation of ROS throughout the leaf, which results into the exit from cell proliferation and the initiation of endoreduplication. The increased endoreduplication rate will result in a higher nuclear ploidy level. Based on this reasoning, Xue et al. (2015) conclude that the *ccr1* dwarfed phenotype is not the result of the reduced lignin content but, instead, is the consequence of the dramatically increased levels of ferulic acid that keep the cellular oxidation state low, resulting in a prolonged phase of cell proliferation, a lower average nuclear ploidy level, and dwarfism (Xue et al., 2015). In the *ccr1-6 ProSNBE:CCR1* lines, *CCR1* expression is only partially restored in vessels. In these lines, all other cells, including leaf mesophyll cells, are still deficient in CCR1. As a consequence, *ccr1-6 ProSNBE:CCR1* lines accumulate ferulic acid to levels similar to those in *ccr1-6*, but only the latter has a prolonged cell proliferation stage and stunted growth. Thus, our results suggest that high levels of ferulic acid are not the reason for the cell cycle

defects and stunted growth of *ccr1* mutants. However, irrespective of its cause, the fact that endoreduplication is restored in *ccr1-6 ProSNBE:CCR1* plants could still indicate that the biomass yield penalty observed in *ccr1-6* mutants is the consequence of the disturbed endoreduplication itself. Interestingly, high endopolyploidy was shown to be associated with increased leaf size in mapping populations (Gegas et al., 2014). Furthermore, the link between endoreduplication and dwarfism of cell wall mutants was made before: the stunted growth of an *esk1-5* mutant, which is impaired in the acetylation of hemicellulose, could be largely suppressed by mutating the *KAKTUS* gene (Bensussan et al., 2015). The latter is described as an endoreduplication repressor and could control cell enlargement in different tissues.

The Yield Penalty of Low-Lignin Mutants Can Be Fully Overcome without Settling in Sugar Yield by Sufficiently Reinforcing the Vessels

Previous vessel-complementation attempts using *VND6* and *VND7* promoter sequences did not achieve a full restoration of vessel integrity and growth while maintaining the high sugar yield for Arabidopsis plants mutated in genes involved in lignin and hemicellulose biosynthesis (Petersen et al., 2012; Yang et al., 2013; Vargas et al., 2016). This could be the consequence of (1) the targeted cell wall biosynthesis gene or (2) the expression level and pattern conferred by the chosen promoter. *VND6* expression is restricted to the metaxylem vessels, whereas *VND7* has the highest expression level in protoxylem vessels (Kubo et al., 2005; Zhong et al., 2008). *ProSNBE* is a target of both VND6 and VND7 and confers expression in both the metaxylem and protoxylem (Zhong et al., 2010; McCarthy et al., 2011). The latter was sufficient to fully restore vessel integrity in *ccr1 ProSNBE:CCR1* stems and leaves, as judged here from the open vessels in the xylem and the appearance of the cell wall observed by light microscopy and transmission electron microscopy. Despite having many characteristics that were similar to *ccr1*, restoration of vascular integrity was sufficient to restore the total plant biomass in *ccr1 ProSNBE:CCR1* lines. These data suggest that the *irx* phenotype of *ccr1* mutants is responsible for their
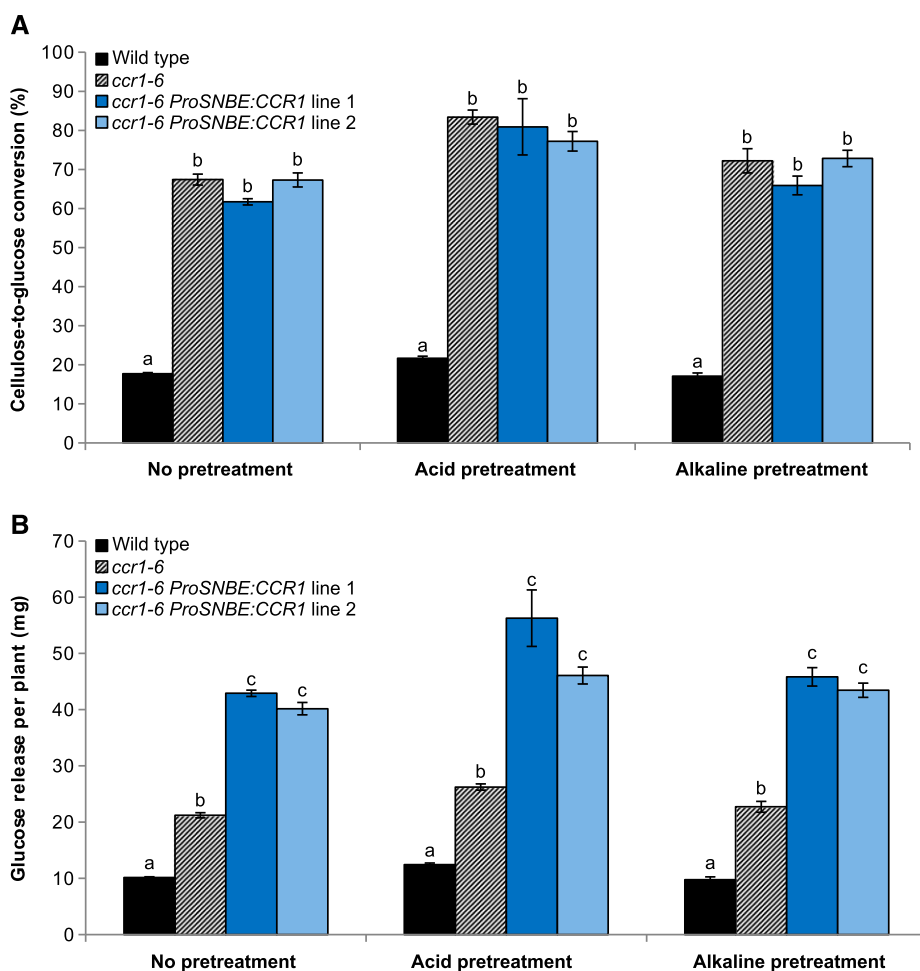
Figure 10. Saccharification efficiency of *ccr1-6 ProSNBE:CCR1* plants. A, Cellulose-to-glucose conversions after 192 h of saccharification of senesced inflorescence stems of the wild type, *ccr1-6*, and *ccr1-6 ProSNBE:CCR1*. B, Glucose release after 192 h of saccharification per total stem biomass. Samples were saccharified using no pretreatment, acid pretreatment (1 M HCl), or alkaline pretreatment (62.5 mM NaOH). Error bars indicate SE; $n = 6$. Different letters represent significant differences at the 0.01 significance level (Dunnett-Hsu adjusted Student's *t* test) per pretreatment.

dwarfed growth and possibly at the origin of the observed cell cycle defect. Additional proof for the collapsed vessel hypothesis as the reason for the dwarfism of cell wall mutants was given by the analysis of other cell wall-modified plants. Arabidopsis cell wall mutants that displayed collapsed vessels (e.g. *ccr1*, *cse*, *c3h1*, *c4h*, *hct*, and *pal1/2/3/4* mutated in lignin biosynthesis; *irx1*, *irx2*, and *irx3* mutated in cellulose biosynthesis; and *irx7*, *irx8*, and *irx9* mutated in xylan biosynthesis) all suffer from growth perturbations (Jones et al., 2001; Franke et al., 2002; Besseau et al., 2007; Huang et al., 2010; Vanholme et al., 2013b; Yang et al., 2013). Moreover, vessel integrity seems to be correlated directly with plant growth. For example, *ccr1-6* mutants and *cad-c cad-d* double mutants have been shown to have similarly decreased lignin contents, but only *ccr1-6* suffered from collapsed vessels and prominent developmental defects (Thévenin et al., 2011). These observations are probably the consequence of the differences in lignin composition providing strength to the vessels: whereas lignin of *ccr1-6* mutants had an S/G ratio of 0.48, *cad-c cad-d* double mutants had an S/G ratio of 0.081. Furthermore, despite the fact that the lignin amount of *med5a med5b c3h* triple mutants was restored to wild-type levels, they still suffered from collapsed vessels and were only partially restored in growth (Bonawitz et al., 2014). In the latter case, it is conceivable that the lignin of *med5a med5b c3h*, which consists mainly of H units and shorter lignin chains, does not provide sufficient strength to the vessels in order to avoid their collapse. In conclusion, we hypothesize that the dwarfism of cell wall mutants can be fully overcome by sufficiently reinforcing the vessels, thereby avoiding their collapse, by optimizing the cell wall composition.

When compared with the wild type, the *ccr1 ProSNBE:CCR1* plants were fully recovered in height, but they also showed an increased number of secondary inflorescences and stem biomass. The increase in secondary inflorescences was also observed for *ccr1-6* mutants and other CCR1-deficient Arabidopsis plants (Goujon et al., 2003; Van Acker et al., 2013). Here, experiments with *ccr1-6 ProSNBE:CCR1*, *ccr1-6*, and the wild type that were not allowed to set seeds showed that the increase in stem biomass in *ccr1-6 ProSNBE:CCR1* lines resulted (largely) from their reduction in seed yield. The latter is supported by the fact that other plants perturbed in silique development (e.g. *ms1-1* and *ap3-1*) also produce more axillary branches (Hensel et al., 1994; Wuest et al., 2016). Moreover, field-grown *ccr1* maize (*Zea mays*) mutants, which also suffered from reduced seed weights, produced significantly more stem biomass when compared with wild-type maize plants (Smith et al., 2017a). The underlying signal leading to an increased biomass in seed-compromised plants remains largely unknown. Elucidation of this signal could open an interesting avenue to increase lignocellulosic biomass and, thus, fermentable sugar yield.

Cellulose-to-glucose conversions of *ccr1-6* and *ccr1-6 ProSNBE:CCR1* lines were 4-fold higher than those of the wild type, independent of the pretreatment. Given the negative correlation between saccharification and lignin amount, the increase in saccharification yield observed in these lines could be largely attributed to the reduced amount of lignin but possibly also to the increased levels of ferulic acid and H units (Ziebell et al., 2010; Van Acker et al., 2013). On a plant basis and compared with the wild type, the total plant sugar yield from the dwarfed *ccr1-6* mutants was increased by 2-fold, whereas the *ccr1-6 ProSNBE:CCR1* lines exhibited a 4-fold increase. The latter is the consequence of the full recovery in height and the increased stem biomass in *ccr1-6 ProSNBE:CCR1* lines when compared with the wild type. To our knowledge, the *ccr1-6 ProSNBE:CCR1* lines are the highest sugar-yielding Arabidopsis lines reported so far.

Potential of the Vessel-Specific Lignin Biosynthesis Strategy To Be Translated into Crops

In addition to their high sugar yield, the *ccr1-6 ProSNBE:CCR1* lines do not suffer from a yield penalty, which makes the translation of this research into biomass crops attractive. Hybrid poplar shows great potential as a woody energy crop (Carroll and Somerville, 2009), and wood of *CCR* down-regulated poplar had up to 161% increased ethanol yield per unit of biomass (Van Acker et al., 2014). However, this strategy resulted in unstable down-regulation of the *CCR* gene and significant yield penalties in the respective trees. Since we have proven that the yield penalty of low-lignin *ccr1* mutants can be fully overcome by allowing sufficient lignification to occur in the cell walls of vessels, a similar approach could be used for the yield recovery of poplar. For example, the stability problem of the down-regulation can be overcome by making stable *ccr* mutants using the efficient CRISPR/Cas9 genome-engineering technique (Tsai and Xue, 2015; Zhou et al., 2015). Recovery of the yield penalty could be achieved by reintroducing *CCR* expression specifically in the vessels. However, because we have proven that, in Arabidopsis, vessels provide monolignols to (xylary) fibers in order to lignify their cell wall, also in poplar the vessels may act as good neighbors to the surrounding fiber cells, as was hypothesized before (Gorzsás et al., 2011). Nevertheless, in Arabidopsis, the vessels were only able to recover the lignin amount in the xylem cells to approximately half that of the wild type. For this reason, a stable reduction in the lignin amount of poplars can potentially be achieved without the corresponding yield penalty. Potential alternative approaches to achieve vessel-specific lignification in poplar is via perturbing the lignification specifically in fibers. Because poplars do not (normally) flower when grown in short rotation for biomass, it is unlikely that they will also show an increase in lignocellulosic biomass, as was observed for the *ccr1 ProSNBE:CCR1* lines. However, translation of this strategy into biomass crops that set seeds but of which the seeds are not the prime target (such as switchgrass [*Panicum virgatum*]) could potentially result in an increased lignocellulosic biomass yield.

MATERIALS AND METHODS

Plant Material and Vector Construction

Arabidopsis (*Arabidopsis thaliana*; ecotype Columbia-0) wild-type, *ccr1-3* (SALK_123689), and *ccr1-6* (GABI_622C01) mutant plants were used as controls and for plant transformation (Mir Derikvand et al., 2008; Ruel et al., 2009; Vanholme et al., 2012; Van Acker et al., 2013). The artificial *SNBE* promoter contained three copies of *XCP1-SNBE1* fused to the CaMV *35S* minimal promoter (from −46 to −1), as described by McCarthy et al. (2011; Supplemental Table S6). To clone this synthetic promoter, the 103-bp construct was first synthesized by Invitrogen (Life Technologies). Next, the construct was PCR amplified using primers containing the restriction sites for *Bam*HI and *Xho*I (Supplemental Table S6). Subsequently, the PCR product was cloned into the Gateway *pEN-L4-R1* vector using T4 DNA Ligase (Invitrogen) to generate the *ProSNBE* entry vector *pEN-L4-ProSNBE-R1*, whose identity was confirmed by sequencing. For the *GFP* and *GUS* reporter line, the *ProSNBE* building block was introduced into the destination vector *pMK7S*NFm14GW* by using LR Clonase (Invitrogen), which fused *ProSNBE* to a nuclear localization signal: *GFP:GUS* reporter construct, resulting in the *ProSNBE:GFP:GUS* expression clone. By using a nuclear localization signal, the resulting fusion protein would accumulate in the nucleus to higher concentrations than when it would remain in the cytoplasm, making the GFP fluorescence signal more easy to observe using fluorescence microscopy (Chytilova et al., 1999). For complementation, the *ccr1-3* and *ccr1-6* mutants were transformed with the *ProSNBE:CCR1* construct. To this end, the coding sequence of *CCR1* was PCR amplified and cloned into the *pDONR221* vector using BP Clonase (Invitrogen; Supplemental Table S6). The sequence identity was confirmed by sequencing. Subsequently, the two building blocks *pEN-L4-ProSNBE-R1* and *pDONR221-L1-CCR1-L2* were introduced into the destination vector *pK7m24GW-FAST* via Multisite LR Clonase Plus (Invitrogen), which resulted in the *ProSNBE:CCR1* expression clone. All the recombinant plasmids were introduced into *Agrobacterium tumefaciens* strain C58C1 PMP90 by electroporation. After plant transformation using the floral dip method, the identification of transformed seeds was based on kanamycin resistance (*ProSNBE:GFP:GUS* reporter lines) or seed fluorescence (*ccr1 ProSNBE:CCR1* lines; Shimada et al., 2010). For the reporter lines, 30 independent T1 plants were analyzed. For the *ccr1 ProSNBE:CCR1* lines, two independent, single-locus, homozygous T3 lines per *ccr1* background were selected for further analysis.

Reporter Gene Analysis

For the reporter line analysis of the aerial parts, 20 independent, single-locus, homozygous T3 plants were cultivated in soil under short-day conditions (8-h-light/16-h-dark photoperiod, 21°C, and 55% humidity) during 6 weeks, after which they were transferred to long-day conditions (16-h-light/8-h-dark photoperiod, 21°C, and 55% humidity). After 5 and/or 8.5 weeks in long-day conditions, primary inflorescence stems and other plant organs were harvested for GUS analysis. The bottom of the inflorescence stem represents nonelongating internodes, while the top of the inflorescence stem represents elongating internodes.

For inflorescence stem cross sections, the bottom 1 cm of the main stem was removed and the above 3 cm was embedded in 7% (w/v) agarose. Sections of 100 µm thick were made using a vibratome (Campden Instruments) and subsequently stained for the presence of GUS by incubating at 37°C (in the dark) in a staining buffer containing 1 mM 5-bromo-4-chloro-3-indolyl β-D-glucopyranoside sodium salt, 0.5% Triton X-100, 1 mM EDTA, pH 8, 0.5 mM potassium ferricyanide, 0.5 mM potassium ferrocyanide, and 500 mM sodium phosphate buffer, pH 7. The staining was performed for 2 h (Fig. 1; Supplemental Fig. S1) or overnight (Supplemental Fig. S1) and subsequently stopped by replacing the staining buffer with 70% (v/v) ethanol (overnight). Next, the sections were transferred to tap water and imaged using a Zeiss Axioskop 2 microscope with an EC Plan-Neofluar 20× (0.5 dry) objective.

For the other aerial organs, plant material was placed in GUS staining solution (as described above), vacuum infiltrated for 1 min, and incubated subsequently overnight at 37°C (in the dark). To terminate the reaction, the staining solution was removed, and plants were incubated overnight in 70% ethanol. Next, the organs were incubated for 1 week in GUS destaining solution (50% glycerol, 25% lactic acid, and 25% Milli-Q water). Images were obtained using a Nikon AZ100M microscope with AZ Plan Apo 0.5× (0.05) objective.

For reporter line analysis of the root, 10 independent, single-locus, homozygous T3 plants were grown for 20 d in long-day conditions on one-half-strength Murashige and Skoog plates. Then, root cell walls were stained with 30 mM propidium iodide at the onset of the experiment. The excitation energy

of 488 nm was from an argon laser. The propidium iodide fluorescence emission was collected between 550 and 650 nm, and GFP fluorescence emission was collected between 500 and 550 nm. All images were captured with an inverted LSM 710 META confocal microscope equipped with 20×-Air objectives (Zeiss).

Plant Growth and Harvest

Unless mentioned otherwise, plants were grown as follows. The *ccr1 ProSNBE:CCR1* lines and their respective controls (the wild type and *ccr1-3* or *ccr1-6*) were cultivated in soil under short-day conditions during 6 weeks, after which they were transferred to long-day conditions. After 4 weeks in long-day conditions, main stems were harvested for lignin microscopy and bending tests, whereas after 5 weeks in long-day conditions, main stems were harvested for metabolic profiling (with plants having a height of approximately 26 cm for *ccr1* and 50 cm for the other lines). For all other analyses, fully senesced plants/stems were used.

For the analysis of the first leaves, two *ccr1-6 ProSNBE:CCR1* lines, the wild type, and *ccr1-6* mutants were grown on soil in long-day conditions. Leaf 1 and leaf 2 were harvested 15 and/or 25 d post stratification.

Biomass Measurements

Plants were fully senesced, on average, after 6 weeks in short-day conditions followed by 10 weeks in long-day conditions. A first set of plants with *ccr1-3*, *ccr1-3 ProSNBE:CCR1*, and their wild-type control and a second set with *ccr1-6*, *ccr1-6 ProSNBE:CCR1* lines, and their wild-type control were grown in two independent experiments. The inflorescence of completely senesced plants was harvested in full. First, the primary inflorescence stem (the main stem) was obtained by stripping off the leaves, axillary inflorescences, and siliques, after which the weight and height were determined and the number of secondary (axillary) inflorescence stems originating from the rosette and directly from the main stem were counted. Second, the secondary inflorescence weight was determined by stripping off the leaves and siliques. Third, seeds of the full plant were harvested for number and weight determinations. The total stem biomass is defined here as the weight of the primary and secondary inflorescences, without seeds, siliques, and leaves. The total plant biomass is defined here as the weight of the harvested aerial part of the plant, including the seeds, siliques, and cauline leaves, but without the rosette leaves.

For the biomass measurements on plants of which the developing siliques were repeatedly removed, the plants were grown as described above. With a frequency of three times per week, all siliques were removed from all plants. When the plants were fully senesced (after, on average, 6 weeks in short-day conditions and 10 weeks [for the control] and 14 weeks [for the plants of which the siliques were removed] in long-day conditions), the number of secondary inflorescence stems originating from the rosette and main stem was determined, after which the total stem biomass was determined.

Two-Point Bending Tests

Bending tests were carried out on 7-cm-long basal segments of primary inflorescence stems. To reduce the effect of turgor loss, stems were tested within 5 min of being harvested. The average cross-sectional area of the stem piece (A) was estimated by considering the cross section as a perfect circle using the formula $A = \pi.(D/2)^2$. Here, D is the average of the diameter measured with a caliper at the basal and at the apical sides of the 7-cm piece. Approximately 2 cm of the basal side of the stem was taped to a support, to keep the stem in a horizontal position. Then, a weight (here, 0.001 kg) was attached to the apical side, after which the vertical deformation of the stem was measured. The bending modulus (Pa) was calculated as $(F.L)/(A.\Delta x)$, where F is the force exerted by the weight on the stem segments (here, F = m. g = 0.0099 N), L is the distance between the support and the position of the weight (here, L = 0.05 m), A (m^2) is the cross-sectional area through which the force is applied, and Δx (m) is the vertical displacement of the stem as a consequence of the applied force.

Light and Fluorescence Microscopy

After removing the bottom 1 cm of the main stem, the above 3 cm was embedded in 7% (w/v) agarose, and slices of 100 µm thick were made using a vibratome (Campden Instruments). Lignin staining with Wiesner and Mäule reagents was performed as described by Sundin et al. (2014). Images were acquired using a Zeiss Axioskop 2 microscope with an EC Plan- Neofluar 20× (0.5

dry) objective. Lignin autofluorescence was imaged using the Zeiss LSM 780 microscope with a Plan-Apochromat 10× (0.45 M27) objective. The fluorescence signal for lignin was obtained using 350 nm for excitation and the emission wavelength ranging from 407 to 479 nm.

For microscopy on 25-d-old first leaves, the harvested leaves were cut into small pieces and immersed in a fixative solution of 2.5% glutaraldehyde and 4% formaldehyde in 0.1 M sodium cacodylate buffer, placed in a vacuum oven for 30 min, and then left rotating for 3 h at room temperature. This solution was later replaced with fresh fixative, and samples were left rotating overnight at 4°C. After washing, samples were postfixed in 1% OsO_4 with potassium ferricyanide in 0.1 M sodium cacodylate buffer, pH 7.2. Samples were dehydrated through a graded ethanol series, including a bulk staining with 2% uranyl acetate at the 50% ethanol step, followed by embedding in Spurr's resin. Semithin sections were cut at 0.5 μm using the Leica EM UC6 ultramicrotome (Leica Microsystems) and stained with Toluidine Blue. Images were acquired using a Zeiss Axioskop 2 microscope with a Plan-Neofluar 100× Ph 3 (1.25 oil)objective.

Transmission Electron Microscopy

After removing the bottom 1 cm of the main stem, the above 3 cm was fixated, dehydrated, and embedded in Spurr's resin as described above for the first leaves. Ultrathin sections of a gold interference color were cut using the Leica EM UC6 ultramicrotome, followed by poststaining with uranyl acetate and lead citrate in the Leica EM AC20, and collected on formvar-coated copper slot grids. They were viewed with the JEM-1400plus transmission electron microscope (JEOL) operating at 60 kV.

Raman Microscopy

After removing the bottom 1 cm of the main stem, the above 3 cm was embedded in polyethylene glycol matrix as described previously ($n = 3$; Gierlinger et al., 2012). Next, 18-μm-thick cross sections were cut using a rotary microtome (Leica RM2255). After polyethylene glycol was removed by rinsing with water, the samples were placed with a drop of water on a glass slide and sealed with a coverslip and nail polish. For each biological replicate, one cross section was analyzed using a confocal Raman microscope (InVia) equipped with a linearly polarized red laser ($\lambda = 633$ nm). A 100× oil-immersion lens was used for high spatial resolution. On each cross section, four Raman mappings were conducted: two in the xylem region and two in the interfascicular region. For the mapping, full spectra were obtained with a 0.3-μm step size. The integration time of one spectrum was set to 3 s using 1,800 I mm^{-1} grating and 18-mW laser power. After data acquisition, a cosmic ray removal was applied using Wire software (Renishaw; version 3.7). The Raman spectra were further analyzed using Cytospec software (Cytospec; version 2.00.01). By integrating the intensity of the band in the range of 1,550 to 1,650 cm^{-1} (which is assigned to the aromatic skeletal vibrations), cell corners, middle lamella, and secondary cell walls could be distinguished. Then, a more detailed region-of-interest study was performed on the secondary cell wall of vessels, xylary fibers, and interfascicular fibers. Three regions of interest were chosen for each anatomical region on each mapping, and an average spectrum was calculated for each region of interest. Consequently, a total number of 18 average spectra was obtained for each anatomical region (vessels, xylary fibers, and interfascicular fibers) of each genotype. The average spectra were then baseline corrected and analyzed further using the software Opus (Bruker; version 7).

Metabolic Profiling

After removing the bottom 1 cm of the stem, the next 11 cm from the bottom of the stem was frozen and ground. Subsequently, the stem tissue was extracted in 2-mL tubes at 70°C by shaking for 15 min with 1 mL of methanol. After centrifugation, the supernatant was transferred to new 1.5-mL tubes and lyophilized. Subsequently, the pellet was resuspended in equal volumes of cyclohexane and ultrapure water (100 μL each). After vortexing, samples were centrifuged, and the aqueous phase was subjected to UHPLC-MS on a Waters Acquity UHPLC device connected to a Synapt HDMS Q-TOF mass spectrometer (Waters). In the chromatograms of the wild type, *ccr1-6*, and the *ccr1-6 ProSNBE:CCR1* lines, a total of 9,746 peaks were processed with Progenesis QI software version 2.1 (Waters), as described by Vanholme et al. (2013b). For peak selection, the following filters were applied: (1) retention time greater than 2 min, (2) value greater than 0 for at least all replicates in one line, and (3)

average peak intensity greater than 5,000 for at least one line. After this, 554 peaks were retained for further PCA and statistical analysis. PCA (autoscaling) was performed in MetaboAnalyst (MetaboAnalyst software version 3.0; Xia and Wishart, 2016). For statistics, a one-way ANOVA was performed on arcsinh-transformed peak areas, which resulted in a list of 274 peaks that were significantly different between at least two lines ($P < 0.001$). Additional posthoc Student's *t* tests were used to find peaks with significantly different peak areas in the *ccr1-6 ProSNBE:CCR1* lines as compared with those in the wild type and in the *ccr1-6* mutants. Peaks that had $P < 0.01$ and a ratio of at least 2-fold (greater than 2 or less than 0.5) when compared with the wild type and/or *ccr1-6* were considered as statistically significant. Another posthoc Student's *t* test showed that there were no significant differences ($P < 0.001$) in peak intensity between *ccr1-6 ProSNBE:CCR1* line 1 and line 2 for these peaks. Therefore, the two *ccr1-6 ProSNBE:CCR1* lines were treated as one line for subsequent analyses. In total, 232 peaks were selected and classified into eight different groups (Fig. 6). The peaks that were significantly different as compared with both the wild type and *ccr1-6* were classified accordingly in groups 1, 3, 6, and 8. Those that were only significantly different from the wild type were reclassified at milder cutoff values when compared with *ccr1-6*: P of 0.05 irrespective of the fold change. As such, additional compounds were classified in groups 1, 3, 6, and 8. Similarly, peaks that were only significantly different as compared with *ccr1-6* were reclassified at milder cutoff values when compared with the wild type: P of 0.05 irrespective of the fold change. Again, additional compounds were classified in groups 1, 3, 6, and 8. The remaining peaks were classified accordingly into groups 2, 4, 5, and 7. Structural characterization was initially performed by matching *m/z*, retention times, and MS/MS fragmentation against our in-house library, created by Instant Jchem for Excel software (Chemaxon). Structural characterization of the remaining unknown compounds was done manually by comparing *m/z* and MS/MS fragmentation with those of compounds described in the literature and online databases.

For the analysis of the first leaves, two different sets of plants were grown to be harvested 15 and 25 d post stratification. During harvesting, the first leaves (leaves 1 and 2) originating from the same plant were pooled together and used further as one sample for metabolite extraction. Hereby, the frozen ground tissue was extracted in 2-mL tubes at 70°C by shaking for 15 min with 500 μL of methanol. After centrifugation, the supernatant was transferred to new 1.5-mL tubes and the methanol was evaporated. Subsequently, the pellet was resuspended in equal volumes of cyclohexane and ultrapure water (75 μL each). After vortexing, samples were centrifuged, and the aqueous phase was analyzed using UHPLC-MS. UHPLC was performed on an ACQUITY UPLC I-Class system (Waters) consisting of a binary pump, a vacuum degasser, an autosampler, and a column oven. Chromatographic separation was carried out on an ACQUITY UPLC BEH C18 (150 × 2.1 mm, 1.7 μm) column from Waters, and temperature was maintained at 40°C. A gradient of two buffers was used: buffer A (99:1:0.1 water:acetonitrile:formic acid, pH 3) and buffer B (99:1:0.1 acetonitrile:water:formic acid, pH 3), as follows: 95% A for 0.1 min decreased to 50% A in 30 min. The flow rate was set to 0.35 mL min^{-1}, and the injection volume was 10 μL. The UHPLC system was coupled to a Vion IMS QTOF hybrid mass spectrometer (Waters). The LockSpray ion source was operated in negative electrospray ionization mode under the following specific conditions: capillary voltage, 2.5 kV; reference capillary voltage, 2.5 kV; cone voltage, 30 V; source offset, 50 V; source temperature, 120°C; desolvation gas temperature, 400°C; desolvation gas flow, 600 L h^{-1}; and cone gas flow, 50 L h^{-1}. The collision energy for full MS was set at 6 eV; for MS/MS (data-dependent analysis) purposes, the collision energy was ramped from 10 to 15 eV for low mass and from 20 to 50 eV for high mass. Nitrogen (greater than 99.5%) was employed as desolvation and cone gas. Leucin-enkephalin (250 pg μL^{-1} solubilized in water: acetonitrile 1:1 [v/v], with 0.1% formic acid) was used for the lock mass calibration, with scanning every 2 min at a scan time of 0.1 s. Profile data were recorded through a UNIFI Scientific Information System (Waters). Data processing was performed with Progenesis QI software version 2.1 (Waters) as described by Vanholme et al. (2013b). After targeted selection of the ferulic acid coupling products, the following filters were applied: (1) value greater than 0 for at least all replicates in one line, (2) average peak intensity greater than 2 for at least one line, and (3) average peak intensity greater than 2 for at least one line. After performing a one-way ANOVA on arcsinh-transformed peak areas ($P < 0.001$), a posthoc Student's *t* test showed that there were no significant differences ($P < 0.001$) in peak intensity between *ccr1-6 ProSNBE:CCR1* line 1 and line 2 for the selected peaks. Therefore, the two *ccr1-6 ProSNBE:CCR1* lines were treated as one line for subsequent statistical analysis. Additional posthoc Student's *t* tests were used to find significant differences between the wild type, *ccr1-6*, and *ccr1-6 ProSNBE:CCR1* ($P < 0.01$). Structural characterization was done as described above for stem samples.

Flow Cytometry

Leaves 1 and 2 were harvested and snap frozen in liquid nitrogen 15 and 25 d post stratification for a first and second set of plants, respectively. Subsequently, 15-d-old leaves were pooled in pairs, whereas 25-d-old leaves were analyzed individually. First, the leaves were chopped with a razor blade. Second, the nuclei were isolated by adding 200 μL of Cystain UV Precise P nuclei extraction buffer and stained using 800 μL of Cystain UV Precise P staining buffer (Sysmex-Partec) before filtering using a 30-μm mesh. Flow cytometry was performed using a Cyflow flow cytometer (Sysmex-Partec), and the results were analyzed using Cyflogic software version 1.2.1 (Cyflogic).

Cell Wall Characterization and Saccharification

For the wild type and *ccr1 ProSNBE:CCR1* lines, the bottom 36 cm of the main stem was chopped into pieces of 2 mm, and samples were pooled per three individuals. For the *ccr1-6* mutants, the bottom 18 cm of the main stem was chopped into pieces of 2 mm, and samples were pooled per six individuals. Preparation of cell wall residue, cellulose quantification, and thioacidolysis were performed as described previously by Van Acker et al. (2013). Saccharification assays were performed as described by Van Acker et al. (2016). For the latter, measurements were performed at different time points after adding the saccharification enzymes: 3, 7, 24, 48, and 197 h. In case of no pretreatment, an extra time point at 97 h was added to obtain more resolution. To calculate the total plant sugar yield, the saccharification efficiency of the primary inflorescence stem was used as representative for all inflorescences. Lignin content was measured using a modified Klason method (Van den Bosch et al., 2015), where the 4-h incubation with a soxhlet extractor was replaced by a 1-h incubation at 121°C in an autoclave.

Supplemental Data

The following supplemental materials are available.

Supplemental Figure S1. GUS expression analysis in growing and senescing *ProSNBE:GFP:GUS* inflorescence stems.

Supplemental Figure S2. Lignin deposition in inflorescence stems of *ccr1-3 ProSNBE:CCR1* lines.

Supplemental Figure S3. Raman microscopy analysis of vessels, xylary fibers, and interfascicular fibers.

Supplemental Figure S4. MS/MS spectra of the 82 putatively structurally characterized metabolites with differential abundance between *ccr1-6 ProSNBE:CCR1* and the wild type or *ccr1-6 ProSNBE:CCR1* and *ccr1-6*.

Supplemental Figure S5. Phenotype of *ccr1-6 ProSNBE:CCR1* seedlings.

Supplemental Figure S6. Impact of *ProSNBE:CCR1* expression in *ccr1-6* mutants on vascular integrity in leaves.

Supplemental Figure S7. Cellulose-to-glucose conversion during saccharification of the senesced inflorescence stems of the wild type, *ccr1-6*, and *ccr1-6 ProSNBE:CCR1* lines.

Supplemental Table S1. Removal of siliques during development results in plants with increased number of secondary inflorescences and higher stem biomass.

Supplemental Table S2. Bending modulus determined by two-point bending tests.

Supplemental Table S3. List of putatively structurally characterized metabolites with different abundance in the inflorescence stems of *ccr1-6 ProSNBE:CCR1* plants as compared with the wild type and/or as compared with *ccr1-6* mutants.

Supplemental Table S4. Mass accuracy of the 82 putatively structurally characterized metabolites.

Supplemental Table S5. Statistical analysis of cellulose-to-glucose conversion efficiencies using different pretreatments.

Supplemental Table S6. Sequence information.

Supplemental Data Set S1. Metabolic profiling data showing the 9,746 peaks detected in wild-type plants, *ccr1-6*, and the *ccr1-6 ProSNBE:CCR1* lines.

LITERATURE CITED

Agarwal UP, Atalla RH (1990) Formation and identification of cis/trans ferulic acid in photoyellowed white spruce mechanical pulp. J Wood Chem Technol **10:** 169–190

Agarwal UP, McSweeny JD, Ralph SA (2011) FT-Raman investigation of milled-wood lignins: softwood, hardwood, and chemically modified black spruce lignins. J Wood Chem Technol **31:** 324–344

Agarwal UP, Ralph SA, Atalla RH (1997) FT Raman spectroscopic study of softwood lignin. *In* 9th International Symposium on Wood and Pulping Chemistry: Proceedings, Montréal, Québec, 1997.

Anderson NA, Bonawitz ND, Nyffeler K, Chapple C (2015) Loss of FERULATE 5-HYDROXYLASE leads to mediator-dependent inhibition of soluble phenylpropanoid biosynthesis in Arabidopsis. Plant Physiol **169:** 1557–1567

Bassard JE, Richert L, Geerinck J, Renault H, Duval F, Ullmann P, Schmitt M, Meyer E, Mutterer J, Boerjan W, De Jaeger G, Mely Y, Goossens A, Werck-Reichhart D (2012) Protein-protein and protein-membrane associations in the lignin pathway. Plant Cell **24:** 4465–4482

Bensussan M, Lefebvre V, Ducamp A, Trouverie J, Gineau E, Fortabat MN, Guillebaux A, Baldy A, Naquin D, Herbette S, et al (2015) Suppression of dwarf and irregular xylem phenotypes generates low-acetylated biomass lines in Arabidopsis. Plant Physiol **168:** 452–463

Besseau S, Hoffmann L, Geoffroy P, Lapierre C, Pollet B, Legrand M (2007) Flavonoid accumulation in *Arabidopsis* repressed in lignin synthesis affects auxin transport and plant growth. Plant Cell **19:** 148–162

Boerjan W, Ralph J, Baucher M (2003) Lignin biosynthesis. Annu Rev Plant Biol **54:** 519–546

Bonawitz ND, Chapple C (2013) Can genetic engineering of lignin deposition be accomplished without an unacceptable yield penalty? Curr Opin Biotechnol **24:** 336–343

Bonawitz ND, Kim JI, Tobimatsu Y, Ciesielski PN, Anderson NA, Ximenes E, Maeda J, Ralph J, Donohoe BS, Ladisch M, et al (2014) Disruption of Mediator rescues the stunted growth of a lignin-deficient *Arabidopsis* mutant. Nature **509:** 376–380

Brown DM, Zeef LAH, Ellis J, Goodacre R, Turner SR (2005) Identification of novel genes in *Arabidopsis* involved in secondary cell wall formation using expression profiling and reverse genetics. Plant Cell **17:** 2281–2295

Carroll A, Somerville C (2009) Cellulosic biofuels. Annu Rev Plant Biol **60:** 165–182

Chen F, Dixon RA (2007) Lignin modification improves fermentable sugar yields for biofuel production. Nat Biotechnol **25:** 759–761

Chen H-C, Li Q, Shuford CM, Liu J, Muddiman DC, Sederoff RR, Chiang VL (2011) Membrane protein complexes catalyze both 4- and 3-hydroxylation of cinnamic acid derivatives in monolignol biosynthesis. Proc Natl Acad Sci USA **108:** 21253–21258

Chytilova E, Macas J, Galbraith DW (1999) Green fluorescent protein targeted to the nucleus, a transgenic phenotype useful for studies in plant biology. Ann Bot (Lond) **83:** 645–654

Cosgrove DJ (2005) Growth of the plant cell wall. Nat Rev Mol Cell Biol **6:** 850–861

Day A, Neutelings G, Nolin F, Grec S, Habrant A, Crônier D, Maher B, Rolando C, David H, Chabbert B, et al (2009) Caffeoyl coenzyme A O-methyltransferase down-regulation is associated with modifications in lignin and cell-wall architecture in flax secondary xylem. Plant Physiol Biochem **47:** 9–19

Del Carmen Martínez-Ballesta M, Moreno DA, Carvajal M (2013) The physiological importance of glucosinolates on plant response to abiotic stress in *Brassica*. Int J Mol Sci **14:** 11607–11625

Eudes A, George A, Mukerjee P, Kim JS, Pollet B, Benke PI, Yang F, Mitra P, Sun L, Çetinkol ÖP, et al (2012) Biosynthesis and incorporation of side-chain-truncated lignin monomers to reduce lignin polymerization and enhance saccharification. Plant Biotechnol J **10:** 609–620

Eudes A, Sathitsuksanoh N, Baidoo EE, George A, Liang Y, Yang F, Singh S, Keasling JD, Simmons BA, Loqué D (2015) Expression of a bacterial

3-dehydroshikimate dehydratase reduces lignin content and improves biomass saccharification efficiency. Plant Biotechnol J 13: 1241–1250

Eudes A, Zhao N, Sathitsuksanoh N, Baidoo EE, Lao J, Wang G, Yogiswara S, Lee TS, Singh S, Mortimer JC, et al (2016) Expression of S-adenosylmethionine hydrolase in tissues synthesizing secondary cell walls alters specific methylated cell wall fractions and improves biomass digestibility. Front Bioeng Biotechnol 4: 58

Franke R, Humphreys JM, Hemm MR, Denault JW, Ruegger MO, Cusumano JC, Chapple C (2002) The Arabidopsis REF8 gene encodes the 3-hydroxylase of phenylpropanoid metabolism. Plant J 30: 33–45

Funk V, Kositsup B, Zhao C, Beers EP (2002) The Arabidopsis xylem peptidase XCP1 is a tracheary element vacuolar protein that may be a papain ortholog. Plant Physiol 128: 84–94

Gegas VC, Wargent JJ, Pesquet E, Granqvist E, Paul ND, Doonan JH (2014) Endopolyploidy as a potential alternative adaptive strategy for Arabidopsis leaf size variation in response to UV-B. J Exp Bot 65: 2757–2766

Gierlinger N, Keplinger T, Harrington M (2012) Imaging of plant cell walls by confocal Raman microscopy. Nat Protoc 7: 1694–1708

Gorzsás A, Stenlund H, Persson P, Trygg J, Sundberg B (2011) Cell-specific chemotyping and multivariate imaging by combined FT-IR microspectroscopy and orthogonal projections to latent structures (OPLS) analysis reveals the chemical landscape of secondary xylem. Plant J 66: 903–914

Goujon T, Ferret V, Mila I, Pollet B, Ruel K, Burlat V, Joseleau JP, Barrière Y, Lapierre C, Jouanin L (2003) Down-regulation of the AtCCR1 gene in Arabidopsis thaliana: effects on phenotype, lignins and cell wall degradability. Planta 217: 218–228

Hensel LL, Nelson MA, Richmond TA, Bleecker AB (1994) The fate of inflorescence meristems is controlled by developing fruits in Arabidopsis. Plant Physiol 106: 863–876

Huang J, Gu M, Lai Z, Fan B, Shi K, Zhou YH, Yu JQ, Chen Z (2010) Functional analysis of the Arabidopsis PAL gene family in plant growth, development, and response to environmental stress. Plant Physiol 153: 1526–1538

Isikgor FH, Becer CR (2015) Lignocellulosic biomass: a sustainable platform for the production of bio-based chemicals and polymers. Polym Chem 6: 4497–4559

Jackson LA, Shadle GL, Zhou R, Nakashima J, Chen F, Dixon RA (2008) Improving saccharification efficiency of alfalfa stems through modification of the terminal stages of monolignol biosynthesis. BioEnergy Res 1: 180–192

Jones L, Ennos AR, Turner SR (2001) Cloning and characterization of irregular xylem4 (irx4): a severely lignin-deficient mutant of Arabidopsis. Plant J 26: 205–216

Kubo M, Udagawa M, Nishikubo N, Horiguchi G, Yamaguchi M, Ito J, Mimura T, Fukuda H, Demura T (2005) Transcription switches for protoxylem and metaxylem vessel formation. Genes Dev 19: 1855–1860

Laskar DD, Jourdes M, Patten AM, Helms GL, Davin LB, Lewis NG (2006) The Arabidopsis cinnamoyl CoA reductase irx4 mutant has a delayed but coherent (normal) program of lignification. Plant J 48: 674–686

Leplé JC, Dauwe R, Morreel K, Storme V, Lapierre C, Pollet B, Naumann A, Kang KY, Kim H, Ruel K, et al (2007) Downregulation of cinnamoyl-coenzyme A reductase in poplar: multiple-level phenotyping reveals effects on cell wall polymer metabolism and structure. Plant Cell 19: 3669–3691

Li E, Bhargava A, Qiang W, Friedmann MC, Forneris N, Savidge RA, Johnson LA, Mansfield SD, Ellis BE, Douglas CJ (2012) The class II KNOX gene KNAT7 negatively regulates secondary wall formation in Arabidopsis and is functionally conserved in Populus. New Phytol 194: 102–115

Mansfield SD, Kang KY, Chapple C (2012) Designed for deconstruction: poplar trees altered in cell wall lignification improve the efficacy of bioethanol production. New Phytol 194: 91–101

Mateu BP, Hauser MT, Heredia A, Gierlinger N (2016) Waterproofing in Arabidopsis: following phenolics and lipids in situ by confocal Raman microscopy. Front Chem 4: 10

McCarthy RL, Zhong R, Ye ZH (2011) Secondary wall NAC binding element (SNBE), a key cis-acting element required for target gene activation by secondary wall NAC master switches. Plant Signal Behav 6: 1282–1285

Meyer MW, Lupoi JS, Smith EA (2011) 1064 nm dispersive multichannel Raman spectroscopy for the analysis of plant lignin. Anal Chim Acta 706: 164–170

Miedes E, Vanholme R, Boerjan W, Molina A (2014) The role of the secondary cell wall in plant resistance to pathogens. Front Plant Sci 5: 358

Mir Derikvand M, Sierra JB, Ruel K, Pollet B, Do CT, Thévenin J, Buffard D, Jouanin L, Lapierre C (2008) Redirection of the phenylpropanoid pathway to feruloyl malate in Arabidopsis mutants deficient for cinnamoyl-CoA reductase 1. Planta 227: 943–956

Mottiar Y, Vanholme R, Boerjan W, Ralph J, Mansfield SD (2016) Designer lignins: harnessing the plasticity of lignification. Curr Opin Biotechnol 37: 190–200

Ohashi-Ito K, Oda Y, Fukuda H (2010) Arabidopsis VASCULAR-RELATED NAC-DOMAIN6 directly regulates the genes that govern programmed cell death and secondary wall formation during xylem differentiation. Plant Cell 22: 3461–3473

Pauly M, Keegstra K (2010) Plant cell wall polymers as precursors for biofuels. Curr Opin Plant Biol 13: 305–312

Persson S, Caffall KH, Freshour G, Hilley MT, Bauer S, Poindexter P, Hahn MG, Mohnen D, Somerville C (2007) The Arabidopsis irregular xylem8 mutant is deficient in glucuronoxylan and homogalacturonan, which are essential for secondary cell wall integrity. Plant Cell 19: 237–255

Pesquet E, Zhang B, Gorzsás A, Puhakainen T, Serk H, Escamez S, Barbier O, Gerber L, Courtois-Moreau C, Alatalo E, et al (2013) Non-cell-autonomous postmortem lignification of tracheary elements in Zinnia elegans. Plant Cell 25: 1314–1328

Petersen PD, Lau J, Ebert B, Yang F, Verhertbruggen Y, Kim JS, Varanasi P, Suttangkakul A, Auer M, Loqué D, et al (2012) Engineering of plants with improved properties as biofuels feedstocks by vessel-specific complementation of xylan biosynthesis mutants. Biotechnol Biofuels 5: 84

Piquemal J, Lapierre C, Myton K, O'Connell A, Schuch W, Grima-Pettenati J, Boudet AM (1998) Down-regulation of cinnamoyl-CoA reductase induces significant changes of lignin profiles in transgenic tobacco plants. Plant J 13: 71–83

Pradhan Mitra P, Loqué D (2014) Histochemical staining of Arabidopsis thaliana secondary cell wall elements. J Vis Exp 2014: 51381

Prinsloo LC, du Plooy W, van der Merwe C (2004) Raman spectroscopic study of the epicuticular wax layer of mature mango (Mangifera indica) fruit. J Raman Spectrosc 35: 561–567

Ralph J, Kim H, Lu F, Grabber JH, Leplé JC, Berrio-Sierra J, Derikvand MM, Jouanin L, Boerjan W, Lapierre C (2008) Identification of the structure and origin of a thioacidolysis marker compound for ferulic acid incorporation into angiosperm lignins (and an indicator for cinnamoyl CoA reductase deficiency). Plant J 53: 368–379

Ruel K, Berrio-Sierra J, Derikvand MM, Pollet B, Thévenin J, Lapierre C, Jouanin L, Joseleau JP (2009) Impact of CCR1 silencing on the assembly of lignified secondary walls in Arabidopsis thaliana. New Phytol 184: 99–113

Serk H, Gorzsás A, Tuominen H, Pesquet E (2015) Cooperative lignification of xylem tracheary elements. Plant Signal Behav 10: e1003753

Shadle G, Chen F, Srinivasa Reddy MS, Jackson L, Nakashima J, Dixon RA (2007) Down-regulation of hydroxycinnamoyl CoA:shikimate hydroxycinnamoyl transferase in transgenic alfalfa affects lignification, development and forage quality. Phytochemistry 68: 1521–1529

Shimada TL, Shimada T, Hara-Nishimura I (2010) A rapid and non-destructive screenable marker, FAST, for identifying transformed seeds of Arabidopsis thaliana. Plant J 61: 519–528

Smith RA, Cass CL, Mazaheri M, Sekhon RS, Heckwolf M, Kaeppler H, de Leon N, Mansfield SD, Kaeppler SM, Sedbrook JC, et al (2017a) Suppression of CINNAMOYL-CoA REDUCTASE increases the level of monolignol ferulates incorporated into maize lignins. Biotechnol Biofuels 10: 109

Smith RA, Schuetz M, Karlen SD, Bird D, Tokunaga N, Sato Y, Mansfield SD, Ralph J, Samuels AL (2017b) Defining the diverse cell populations contributing to lignification in Arabidopsis stems. Plant Physiol 174: 1028–1036

Smith RA, Schuetz M, Roach M, Mansfield SD, Ellis B, Samuels L (2013) Neighboring parenchyma cells contribute to Arabidopsis xylem lignification, while lignification of interfascicular fibers is cell autonomous. Plant Cell 25: 3988–3999

Stout J, Chapple C (2004) The phenylpropanoid pathway in Arabidopsis: lessons learned from mutants in sinapate ester biosynthesis. Recent Adv Phytochem 38: 39–67

Sundin L, Vanholme R, Geerinck J, Goeminne G, Höfer R, Kim H, Ralph J, Boerjan W (2014) Mutation of the inducible ARABIDOPSIS

THALIANA CYTOCHROME P450 REDUCTASE2 alters lignin composition and improves saccharification. Plant Physiol 166: 1956–1971

Taylor NG, Scheible WR, Cutler S, Somerville CR, Turner SR (1999) The *irregular xylem3* locus of *Arabidopsis* encodes a cellulose synthase required for secondary cell wall synthesis. Plant Cell 11: 769–780

Thévenin J, Pollet B, Letarnec B, Saulnier L, Gissot L, Maia-Grondard A, Lapierre C, Jouanin L (2011) The simultaneous repression of CCR and CAD, two enzymes of the lignin biosynthetic pathway, results in sterility and dwarfism in *Arabidopsis thaliana*. Mol Plant 4: 70–82

Tsai CJ, Xue LJ (2015) CRISPRing into the woods. GM Crops Food 6: 206–215

Turner SR, Somerville CR (1997) Collapsed xylem phenotype of *Arabidopsis* identifies mutants deficient in cellulose deposition in the secondary cell wall. Plant Cell 9: 689–701

Van Acker R, Leplé JC, Aerts D, Storme V, Goeminne G, Ivens B, Légée F, Lapierre C, Piens K, Van Montagu MCE, et al (2014) Improved saccharification and ethanol yield from field-grown transgenic poplar deficient in cinnamoyl-CoA reductase. Proc Natl Acad Sci USA 111: 845–850

Van Acker R, Vanholme R, Piens K, Boerjan W (2016) Saccharification protocol for small-scale lignocellulosic biomass samples to test processing of cellulose into glucose. Bio Protoc 6: e1701

Van Acker R, Vanholme R, Storme V, Mortimer JC, Dupree P, Boerjan W (2013) Lignin biosynthesis perturbations affect secondary cell wall composition and saccharification yield in *Arabidopsis thaliana*. Biotechnol Biofuels 6: 46

Van den Bosch S, Schutyser W, Vanholme R, Driessen T, Koelewijn SF, Renders T, De Meester B, Huijgen WJJ, Dehaen W, Courtin C, et al (2015) Reductive lignocellulose fractionation into soluble lignin-derived phenolic monomers and dimers and processable carbohydrate pulps. Energy Environ Sci 8: 1748–1763

Vanholme B, Desmet T, Ronsse F, Rabaey K, Van Breusegem F, De Mey M, Soetaert W, Boerjan W (2013a) Towards a carbon-negative sustainable bio-based economy. Front Plant Sci 4: 174

Vanholme R, Cesarino I, Rataj K, Xiao Y, Sundin L, Goeminne G, Kim H, Cross J, Morreel K, Araujo P, et al (2013b) Caffeoyl shikimate esterase (CSE) is an enzyme in the lignin biosynthetic pathway in *Arabidopsis*. Science 341: 1103–1106

Vanholme R, Demedts B, Morreel K, Ralph J, Boerjan W (2010) Lignin biosynthesis and structure. Plant Physiol 153: 895–905

Vanholme R, Storme V, Vanholme B, Sundin L, Christensen JH, Goeminne G, Halpin C, Rohde A, Morreel K, Boerjan W (2012) A systems biology view of responses to lignin biosynthesis perturbations in *Arabidopsis*. Plant Cell 24: 3506–3529

Vargas L, Cesarino I, Vanholme R, Voorend W, de Lyra Soriano Saleme M, Morreel K, Boerjan W (2016) Improving total saccharification yield

of Arabidopsis plants by vessel-specific complementation of *caffeoyl shikimate esterase* (*cse*) mutants. Biotechnol Biofuels 9: 139

Voelker SL, Lachenbruch B, Meinzer FC, Jourdes M, Ki C, Patten AM, Davin LB, Lewis NG, Tuskan GA, Gunter L, et al (2010) Antisense down-regulation of *4CL* expression alters lignification, tree growth, and saccharification potential of field-grown poplar. Plant Physiol 154: 874–886

Weng JK, Chapple C (2010) The origin and evolution of lignin biosynthesis. New Phytol 187: 273–285

Weng JK, Li X, Bonawitz ND, Chapple C (2008) Emerging strategies of lignin engineering and degradation for cellulosic biofuel production. Curr Opin Biotechnol 19: 166–172

Wilkerson CG, Mansfield SD, Lu F, Withers S, Park JY, Karlen SD, Gonzales-Vigil E, Padmakshan D, Unda F, Rencoret J, et al (2014) Monolignol ferulate transferase introduces chemically labile linkages into the lignin backbone. Science 344: 90–93

Wuest SE, Philipp MA, Guthörl D, Schmid B, Grossniklaus U (2016) Seed production affects maternal growth and senescence in Arabidopsis. Plant Physiol 171: 392–404

Xia J, Wishart DS (2016) Using MetaboAnalyst 3.0 for comprehensive metabolomics data analysis. Curr Protoc Bioinformatics 55: 14.10.11–14.10.91

Xue J, Luo D, Xu D, Zeng M, Cui X, Li L, Huang H (2015) CCR1, an enzyme required for lignin biosynthesis in Arabidopsis, mediates cell proliferation exit for leaf development. Plant J 83: 375–387

Yang F, Mitra P, Zhang L, Prak L, Verhertbruggen Y, Kim JS, Sun L, Zheng K, Tang K, Auer M, et al (2013) Engineering secondary cell wall deposition in plants. Plant Biotechnol J 11: 325–335

Zhong R, Morrison WH III, Negrel J, Ye ZH (1998) Dual methylation pathways in lignin biosynthesis. Plant Cell 10: 2033–2046

Zhong R, Lee C, Ye ZH (2010) Global analysis of direct targets of secondary wall NAC master switches in *Arabidopsis*. Mol Plant 3: 1087–1103

Zhong R, Lee C, Zhou J, McCarthy RL, Ye ZH (2008) A battery of transcription factors involved in the regulation of secondary cell wall biosynthesis in *Arabidopsis*. Plant Cell 20: 2763–2782

Zhou X, Jacobs TB, Xue LJ, Harding SA, Tsai CJ (2015) Exploiting SNPs for biallelic CRISPR mutations in the outcrossing woody perennial *Populus* reveals 4-coumarate:CoA ligase specificity and redundancy. New Phytol 208: 298–301

Ziebell A, Gracom K, Katahira R, Chen F, Pu Y, Ragauskas A, Dixon RA, Davis M (2010) Increase in 4-coumaryl alcohol units during lignification in alfalfa (*Medicago sativa*) alters the extractability and molecular weight of lignin. J Biol Chem 285: 38961–38968